

**I. Earthshine and the Earth's Albedo: Precise and Large-Scale Nightly  
Measurements**

A<sup>1,2</sup>, B<sup>2</sup>, C<sup>3</sup> and D<sup>3</sup>

<sup>1</sup> U1

<sup>2</sup> U2

<sup>3</sup> U3

Received \_\_\_\_\_; accepted \_\_\_\_\_

## ABSTRACT

*Subject headings:* Earth : albedo, global climate — Moon: reflection

Since late 1998 sustained observations of the earthshine have been made from Big Bear Solar Observatory in California. We also have intermittent observations from 1994-5. We have re-invigorated and modernized a nearly forgotten way of measuring the earth's albedo, and hence its energy balance. For about a quarter-century, early in the last century, Danjon and his followers observed the earthshine from France. This is the first in a series of papers covering observations and simulations of the earth's reflectance from photometric and spectral observations of the moon. Here, we develop the modern method of measuring, instantaneously, the large scale reflectance of the earth.

From California, we see the moon reflecting sunlight from the third of the earth to the west of us in our evening – before midnight – which is during the moon's rising phase, and from the third of the earth to our east in our morning – after midnight – which is during the moon's declining phase.

We have precisely measured the scattering from the moon, as a function of lunar phase, which enables us to measure, in a typical night's observations, the earth's reflectance to an accuracy of 2.0% (equivalent to measuring the earth's emission temperature to  $\sim 0.8$  K). The albedo is due to the interplay of cloud cover and the different landscapes.

## 1. Introduction

It is important to know whether there is an on-going global change in the earth’s climate. To answer this, one needs precise, global/integrated measures of relevant quantities. The earth’s climate is driven by the net sunlight deposited in the terrestrial atmosphere, and so, is critically sensitive to the solar irradiance and the earth’s albedo. Precise measurements of the solar irradiance have been made by various satellites and using ground-based proxies (for a review, see Fröhlich, 2000, and references therein). The spectrum of efforts to determine the earth’s global albedo is not so rich. There have been efforts using systems of satellites (Buratti et al., 1997, and references therein), but virtually no efforts from the ground. Nonetheless, the earth’s energy balance is determined in large part by its global albedo – the fraction of the incident sunlight that is directly reflected back into space without altering the internal energy budget of the atmosphere. The earth’s surface, aerosols in the atmosphere, and clouds all reflect some of the incoming solar short-wavelength radiation, preventing that energy from warming the planet. Short-wavelength radiation, usually defined as having wavelengths between 0.15 and 4.0  $\mu\text{m}$ , includes about 99% of the sun’s radiation; of this energy, 46% is infrared ( $> 0.74 \mu\text{m}$ ), 9% is ultraviolet ( $< 0.4 \mu\text{m}$ ) and the remaining 45% is visible, with wavelengths between 0.4 and 0.74  $\mu\text{m}$ . A significant portion of the solar energy is absorbed by the earth, where it drives terrestrial phenomena before being radiated back into space. This long-wavelength radiation peaks at about 15  $\mu\text{m}$  (corresponding to the earth’s black-body temperature of about  $T_E = 255 \text{ K}$ ).

The power going into the earth’s climate system is

$$P_{in} = C\pi R_e^2(1 - A), \tag{1}$$

where  $C$  is the solar constant,  $R_e$  is the earth’s radius and  $A$  is the short-wavelength Bond albedo (reflectance). Similarly, the long-wavelength power that the earth radiates into space is

$$P_{out} = 4\pi R_e^2\sigma\epsilon T_e^4, \tag{2}$$

where  $\sigma$  is the Stefan-Boltzmann constant and  $\epsilon$  is the emissivity of the atmosphere (about 5.5 km

high, where the long-wavelength radiation is emitted).

If the planet is in radiative equilibrium,  $P_{in} = P_{out}$ , and we have

$$T_e^4 = \frac{C}{4\sigma\epsilon}(1 - A). \quad (3)$$

This means that the Bond albedo directly controls the earth’s temperature. Global warming would result if  $A$  and/or  $\epsilon$  decreased. By measuring the earth’s reflectance and the spectrum of the reflected light, one can determine  $A$  and  $\epsilon$ , respectively.

It has been known for some time that the so-called solar constant varies. In particular, data from the Active Cavity Radiometer (ACRIM I) on board the Solar Maximum Mission have shown for one cycle ( $\sim 11$  years) that the solar irradiance is about 0.1% greater at activity maximum than activity minimum (Willson and Hudson 1988, 1991). The precise origin of the changing irradiance is generally attributed to a competition between two components of the sun’s magnetic field – dark sunspots and bright faculae, but an unambiguous description remains elusive. It is conventional wisdom that a 0.1% change is about several times too small to be climatologically significant over a solar cycle (Lean, 1997). It has been argued that there may have been two to three times larger, sustained excursions (Lean, 1997) in the recent past, like during the little ice age when a sunspot was rare. Still, there is strong evidence of a solar cycle going back more than 100,000 years (Ram and Stoltz, 1999). If the 0.1% increase in the mean solar irradiance between the mid-1980s and 1990 were typical, then one is led to consider more carefully the possibility of a variation in the earth’s albedo. After all, the earth’s reflectance is not so well-studied and seems to show considerable variation, Goode et al. (2001).

One might have anticipated that global changes in the earth’s climate would be manifest in changes in the earth’s albedo. Here, we focus on a terrestrial determination of the earth’s global albedo from an old, and largely forgotten method. That is, global albedo can be determined by measuring the amount of sunlight reflected from the earth and in turn, back to the earth from the dark portion of the face of the moon (the “earthshine” or “ashen light”). The most important historical program of earthshine measurements was carried out by Danjon (1928, 1954) from a

number of sites in France. He used a “cat’s-eye” photometer to produce a double image of the moon, allowing the visual comparison of the intensities of two well-defined patches of the lunar surface—one in sunlight and the other in the earthshine—at various lunar phases. Using the “cat’s-eye” mechanism, he stopped-down the light from the sunlit portion to match the brightness of the ashen portion. This differential measurement removed many of the uncertainties associated with varying atmospheric absorption and the solar constant, allowing Danjon to achieve his estimated uncertainty of roughly 5%, ignoring his appreciable systematic error from an incorrect determination of the moon’s reflectivity. Our measurements are about an order of magnitude more precise than his estimates, not simply because we have better cameras available, but we have also solved the problem of the uncertainty in the scattering from the moon as a function of the phase of the moon (see §5). At a better than 1% precision, our terrestrial measurements of the earth’s albedo have a precision comparable to that from satellites.

From 1926 to 1930, Danjon made 207 measurements of earthshine. Dubois (1947) continued the program through 1960 from the observatory at Bordeaux using a Danjon-type photometer.

Danjon’s and Dubois’ results show a number of interesting features. The daily mean values of the observations vary more widely than would be expected on the basis of the variation of measurements on a single night. This can plausibly be attributed to daily changes in cloud cover, but extensive cloud-cover data were not available at the time of the observations.

Danjon (1928) also examined his observations to determine whether there was a long-term trend in albedo, but found none. Dubois’ observations for some 20 years ending in 1960, showed considerable annual variability, which he speculated was due to solar activity. His published monthly variations from 1940-1944 also show a strong correlation with the 1941-42 El Niño. In the past forty years, there have been observations of earthshine by Huffman et al. (1989) and one-time observations by Franklin (1967) and Kennedy (1969).

Danjon used his observations to estimate the mean global albedo. Since the observations are only at visible wavelengths, they must be corrected for the balance of the short-wavelength radiation, most of which is in the near IR. Estimates of this correction were made by Fritz (1949),

after taking into account the decrease of the earth’s albedo with increasing wavelength (our “blue planet”). Fritz also attempted to correct for the geographical bias in Danjon’s observations. The western hemisphere, which was most frequently observed by Danjon, has a greater fraction of land than does the globe as a whole, implying that Danjon’s value would be high because the sea is dark compared to land. Combining the decreases from the absence of the IR and geographical bias, Fritz found that Danjon’s visual albedo of 0.40 corresponds to a Bond albedo (considering all the wavelengths and directions) of 0.36.

Flatte et al. (1991) noted that a correction must be made for the “opposition effect” present in lunar reflectance properties. Observations of the moon show that the moon’s reflectivity has a strong angular dependence. This “lunar phase function” can rise by as much as a factor of two in going from  $5^\circ$  to  $0^\circ$  (exact backscattering). This enhancement was once thought to be due to the porous nature of the lunar surface (Hapke, 1971), and was unknown in Danjon’s time. More modern work has shown it to be caused by coherent backscatter in the lunar soil. The smallest lunar phase angle measured by Danjon was only  $11^\circ$ . The extent of the small-angle rise varies over different regions of the lunar surface, but can easily be the 20% required to reduce Fritz’s value of 0.36 to the generally recognized standard of about 0.30 (Buratti et al., 1997). In fact, we shall see in that an incorrect lunar phase function is the primary source of Danjon’s overly large visual albedo.

We have been steadily observing the earthshine from Big Bear since 1998 to determine the earth’s reflectance and its variations. In this paper, we discuss in detail the method we used to determine reflectance from earthshine. As mentioned, the first such observations were made by Danjon (1928), and considerable modernization was required to make this method sufficiently precise to usefully complement satellite measurements. Beyond developing the methodology, our purpose here is to demonstrate the reliability of the technique. This is the first of a series of papers deriving from our earthshine project. The next two papers will present and interpret the results of our observational work and simulations of the observations. The fourth paper concerns our observations of the spectrum of the earthshine from the 60” telescope on Mt. Palomar.

## 2. Determining the Earth’s Reflectivity from Earthshine

Terrestrial measurements of the short-wavelength (visible light and near infrared) albedo of a planet in our solar system is relatively straightforward – except for the earth. However, we can determine the albedo from the ground by measuring the earthshine. From a terrestrial perspective, the earthshine is the sunlight reflected from the day side of the earth to the moon, and finally back to an observer on the night side of the earth. At any moment, the earthshine can provide an instantaneous, differential cross-section of the sunlight reflected from the earth, see Figure 1.

The earth’s differential cross-section depends on its geometrical albedo and its phase function. The geometrical albedo is independent of  $\beta$ , rather, it is proportional to the backscattered cross-section. At the earth’s surface, the differential cross-section of the reflected sunlight for scattering by an angle  $\beta$  (note that  $\beta$  is the supplement of the usual scattering angle) is given by

$$\frac{d\sigma}{d\Omega} \equiv p_e f_e(\beta) R_e^2, \quad (4)$$

where  $R_e$  is the radius of the earth,  $p_e$  is the geometrical albedo of the earth and  $f_e(\beta)$  is the earth’s phase function, defined such that  $f_e(0) = 1$ , as can be seen in the Lambertian limit from Equation (7).

Using Equation (4), we can write the total scattering cross section as

$$\sigma = \int \frac{d\sigma}{d\Omega} d\Omega = \pi R_e^2 p_e \int_{-\pi}^{\pi} f_e(\beta) |\sin(\beta)| d\beta, \quad (5)$$

where  $p_e$  and  $f_e$  depend on the earth’s weather, season and climate. Additionally,  $f_e$  depends on the earth’s aspect.

From the total cross-section, we can define the Bond albedo – the fraction of solar energy incident on the planet that is reflected as

$$A = \frac{\sigma}{\pi R_e^2} = p_e \int_{-\pi}^{\pi} f_e(\beta) |\sin(\beta)| d\beta. \quad (6)$$

Using earthshine data, we integrate over the phases of the moon to determine, say, a seasonally averaged Bond albedo.  $\beta$  varies between 0 and  $\pm\pi$ , with 0 to  $\pi$  being the waxing moon and  $-\pi$  to 0 being the waning moon.

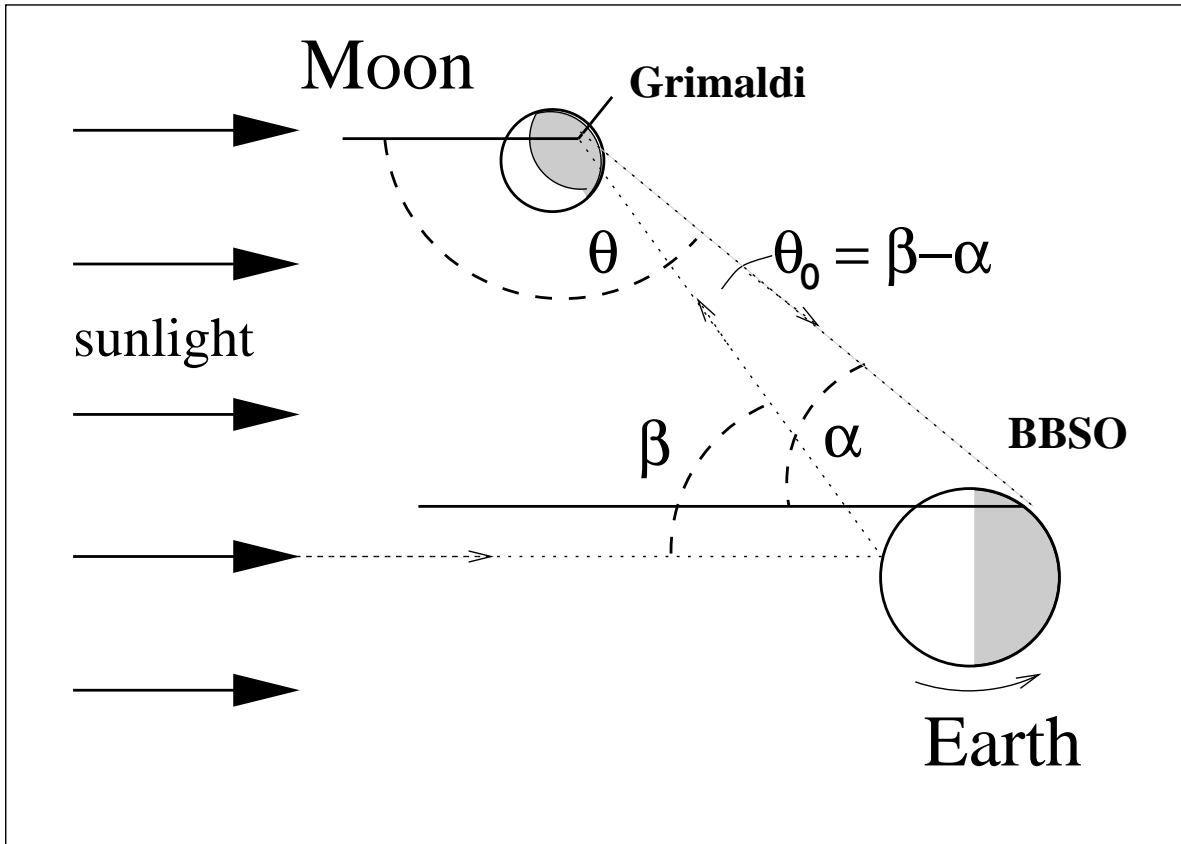


Fig. 1.— A not-to-scale cartoon of the sun-earth-moon system defining the earth’s topocentric phase angle,  $\alpha$ , with respect to BBSO. The plot also shows the moon’s selenographic phase angle,  $\theta$ , with respect to one of the fiducial points (Grimaldi) used in the observations made from BBSO (also indicated).  $\beta$  is the angle between the sunlight that is incident somewhere on the earth and reflected, as earthshine, to Grimaldi.  $\theta_0(= \beta - \alpha)$  is the angle between the earthshine that is incident, and reflected from the moon. The path of the earthshine is indicated by the arrows.  $\theta_0$  is of order  $1^\circ$ , or less.



If we assume that the earth is a Lambert sphere, we can do the integrals in Equations (5) and (6) exactly. A Lambert sphere reflects isotropically from its assumed to be fully diffusive surface.

Then,  $f_L$ , the earth's Lambert phase function, is determined by

$$f_L(\beta) = \frac{(\pi - |\beta|) \cos \beta + \sin |\beta|}{\pi}. \quad (7)$$

The earth's phase function is observed to be very roughly Lambertian for  $|\beta| \leq \frac{2\pi}{3}$ , Goode et al. (2001). Under this assumption, we determine a simple proportionality between the geometric albedo and the global or Bond albedo, namely,

$$p_{e,L} = \frac{2}{3} A_{B,L}. \quad (8)$$

Modelling also shows that the earth's phase function is approximately Lambertian for  $\beta \leq \frac{2\pi}{3}$ .

Thus, a conveniently normalized, differential measure of the earth's reflectivity is the effective albedo,  $A^*$ , where

$$A^* \equiv \frac{p_e f_e}{p_{e,L} f_{e,L}} A_{B,L} = \frac{3 p_e f_e}{2 f_L}, \quad (9)$$

which is the albedo of a Lambert sphere that would give the same instantaneous reflectivity as the true earth at the same phase angle, and where an unchanged  $A^*$  as a function of phase angle would imply a Lambertian earth.

An observer on the moon in the region illuminated by the sun and visible from the earth would see both the direct sunlight and some part of the sunlit earth. The solar intensity seen by that observer would be

$$I_s = \frac{C}{R_{ms}^2}, \quad (10)$$

where  $C$  is the solar constant and  $R_{ms}$  is the moon-sun distance measured in astronomical units.

Similarly, the intensity of the earthlight would be

$$I_e = \frac{C}{R_{es}^2} p_e f_e(\beta) \frac{R_e^2}{R_{em}^2}, \quad (11)$$

where  $R_{ms}$  and  $R_{es}$  are the moon-sun and earth-sun distances, respectively. Thus, the earth's reflectivity can be expressed as

$$p_e f_e(\beta) = \frac{I_e}{I_s} \left[ \frac{R_{em}}{R_e} \right]^2 \left[ \frac{R_{es}}{R_{ms}} \right]^2. \quad (12)$$

In the observations, we study pairs of diametrically opposite fiducial patches, five in the earthshine and the other five in the “moonshine” (sunlight reflected from the moon to the earth) both near the night-time lunar limb. For our purposes here, we call a representative pair “ $a$ ” and “ $b$ ” and treat them as unit projected areas. If  $a$  is illuminated only by the earthshine, the intensity observed by an observer on the earth at a distance  $R_{oa}$  would be

$$I_a = I_e \frac{p_a f_a(\theta_0)}{R_{oa}^2} T_a, \quad (13)$$

where  $T_a$  is the transmission of the earthshine through the atmosphere, and  $f_a(\theta_0)$  is the *lunar* phase function for the near retroreflection from patch  $a$ , see Figure 1. Thus,  $I_a/T_a$  is the observed intensity corrected for airmass. Similar to Equation (13), the intensity of the sunlit portion,  $b$ , would be

$$I_b = I_s \frac{p_b f_b(\theta)}{R_{ob}^2} T_b, \quad (14)$$

where  $\theta$  is the lunar phase angle and  $\theta$ , like  $\alpha$  and  $\beta$ , varies between 0 and  $\pm\pi$ , and where the lunar phase function,  $f_b(\theta)$  embodies the dependence of the fiducial patch on the angle between the sunshine and the moonshine, see Figure (1). Thus,

$$\frac{I_a/T_a}{I_b/T_b} = \frac{I_e p_a f_a(\theta_0)}{I_s p_b f_b(\theta)} \frac{R_{ob}^2}{R_{oa}^2}, \quad (15)$$

and so

$$p_e f_e(\beta) = \frac{I_a/T_a}{I_b/T_b} \frac{p_b f_b(\theta)}{p_a f_a(\theta_0)} \left[ \frac{R_{es}}{R_e} \right]^2 \left[ \frac{R_{oa}}{R_{ob}} \right]^2 \left[ \frac{R_{em}}{R_{ms}} \right]^2. \quad (16)$$

Since  $\frac{I_e}{I_s}$  is independent of lunar phase, Equation (16) is also independent of lunar reflectance provided all quantities labelled by “ $a$ ” are derived from the earthshine and all labelled “ $b$ ” come from moonshine. However, we ultimately take  $p_a$  and  $f_a(\theta_0)$  from moonshine data, which introduces a dependence on the lunar reflectance. This small effect (the effect of 50 Å shift in the spectrum is small compared to the spread among the  $\frac{p_b}{p_a}$ ), and we treat it as being subsumed into that ratio, see §5.4. Also,  $[\frac{R_{oa}}{R_{ob}}]^2$  is so close to unity that we can safely set that factor in Equation (16) to unity. Thus, we determine that

$$p_e f_e(\beta) = \frac{I_a/T_a}{I_b/T_b} \frac{p_b f_b(\theta)}{p_a f_a(\theta_0)} \left[ \frac{R_{em}}{R_e} \right]^2 \left[ \frac{R_{es}}{R_{ms}} \right]^2. \quad (17)$$

We measure  $I_a$  and  $I_b$  in our nightly observations, and correct for airmass (e.g.,  $I_a/T_a$ ). We have measured the lunar phase function quite accurately over the last two years. We use total eclipse data from 93November 29 to measure the ratio of the geometrical cross-sections of the two fiducial patches,  $\frac{p_b}{p_a}$ . For our fiducial regions, this ratio ranges between 0.9 and 1.1. In §6, we combine Equations (9) and (17) to define our measure of the earth’s reflectivity,  $A^*$ , in terms of measured quantities, including the varying earth-moon distance.

### 3. Observations: Earthshine Instrumentation and Data Acquisition

Earthshine observations are currently being carried out at BBSO. The earthshine telescope is aligned with, and mounted atop the 65 cm solar telescope. Figure 2 shows a schematic of the earthshine telescope.

#### 3.1. Hardware

The basic optical components of the earthshine telescope consist of an f/15 telescope primary, which is a 6-inch diameter air-spaced doublet. The telescope tube is attached and aligned with the 65 cm solar telescope, which enables us to use the large telescope’s drive software, permitting tracking following the moon’s variable rate. The tracking rate is updated, via software, every thirty minutes to match the changing lunar motion in the east-west direction. Minor north-south corrections are done with the telescope control paddle as needed during the course of the night’s observations. The moon is initially acquired using a simple two-lens finder scope aligned with the other telescopes on the 65 cm main telescope. The 65 cm telescope is regularly re-balanced for equipment changes so that tracking stability is not a problem even with long exposures. At the end of the tube is a stray light field stop. The incoming moonlight passes the field stop, and then enters a light-tight optical assembly box that holds the filters and camera optics.

In the box, just behind the tube field stop and just before prime focus, is the earthshine neutral density filter switcher. Two filters are placed in the switcher. The first neutral density

filter is a Schott NG3 2mm (the laboratory measured transmission of the filter, used for the first two years of observations, is 0.0115, as a whole, from 4000-7000 Å) for the Bright Side (BS) measurements. The BS or moonshine filter covers the entire field of view and is in place to prevent camera saturation and to provide a reasonably long exposure time (several 100 ms) compared to the smallest exposure time for the camera (10 ms). Thus, to determine the absolute value of the earth’s reflectance, one needs to know precisely the transmission of this filter (§4.3). The second filter is a Schott NG10 2mm (transmission is about  $2 \times 10^{-5}$  over 4000-6000Å), which is essentially a blocking filter to cut off the bright side of the moon to permit the dark side or earthshine (ES) observations. The blocking filter covers the bright side of the moon to permit long, dark side exposures ( $\sim 60$ -150 s) to get optimal signal to noise for the ES images. The blocking filter is carefully placed within the filter holder, by hand, at the beginning of each observing session. Its location, designed to cover the terminator, depends on the phase and libration of the moon. Both filters were scanned to check transmission with wavelength at Gamma Scientific in San Diego using a Radoma spectro-radiometer. Both of these two filters were found to be well within the quoted Schott tolerances.

The prime focus is after the filter holder, and it is closely followed by a flat field lens. Next in the optical train are two near IR filters, which stop any light beyond 7000 Å from reaching the camera. An iris behind the near IR filters acts as a further stray light stop. Behind the iris is a camera lens that focuses the lunar image on the CCD. Between this lens and the camera is a space for a second filter wheel (not shown), which can be used for narrow band measurements. All elements are rail mounted for linear adjustments, and lens elements are in moveable  $y - z$  mountings for fine adjustments. All fine-tuning was done in the Fall of 1998, and nothing has been changed on the system since the start of data acquisition in December 1998. The system was “frozen” to limit possible errors in calibrating the lunar phase function. Flat field images help to point out the location of occasional dust particles that get into the optics. Compressed air removes most particles, and when necessary, elements are removed for cleaning, and then are carefully replaced to preserve optical alignment.

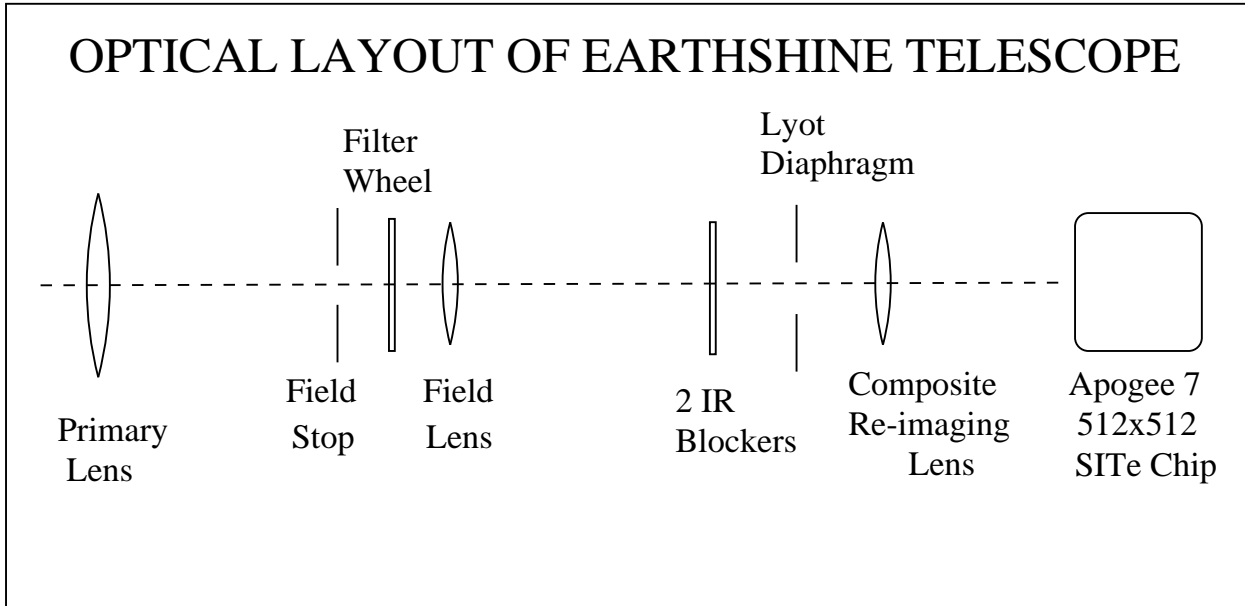


Fig. 2.— The optical set-up of the earthshine telescope.

The CCD camera used in our current earthshine observations is an Apogee 7. The camera is a 512 X 512 16-bit scientific system with a SiTe back-illuminated, thinned silicon chip. This chip, which is one of SiTe’s highest grade, is designed for higher quantum efficiency than unthinned front illuminated chips – this advantage is most apparent toward the blue. One drawback of the higher efficiency SiTe chip is its sensitivity to “after-images” caused by exposure to UV. Testing the earthshine system to limit this effect resulted in the following observing procedures: 1) The UV from the BS images is reduced by the BS (NG3) filter. 2) The worst after-images show up in the ES images on the unfiltered half of the image – which are of long exposure. It was found that a series of subsequent, short BS images, the UV residual image was removed before the next long earthshine exposure. 3) Careful examination of dark current and flat field images taken during the course of observations is done to confirm this, night by night.

Initial testing demonstrated a linear response over the camera’s entire 16-bit range. To check for change in the camera’s response with time, a calibrated radiometer was purchased to check the camera’s response during each new moon. Dome flats are taken in varying illumination to get pixel count versus intensity. The radiometer is an IL 1700, a NIST traceable Silicon photodiode

radiometer. Once a year, the radiometer will be returned to International Light for re-calibration.

### 3.2. Observations

After initial tests, our current round of earthshine observations began in November 1998. A typical raw image is shown in Figure 3. The five pairs of fiducial patches used in the data reduction (see §4) are also indicated. The camera’s graphic user interface, in C code, was supplied by the manufacturer, and it was modified to efficiently handle the routine earthshine observations. The nightly observations follow a simple set of procedures, which are mostly automated. During the course of observations BS, ES, dark current, and flat field images are taken regularly.

The first 8 months of observations covered lunar phases between  $0^\circ$  and  $\pm 140^\circ$ , which is about 21 days a month. The initial observation over this wide range of phases was necessary to determine the lunar phase function and prove its repeatability. During the first 8 months, for the phases near the full moon ( $-40^\circ$  through  $0^\circ$  to  $+40^\circ$ ), ES images were not taken because both fiducial patches were in, or so near to sunlight that ES measurements were unreliable. On these nights only BS, dark current, and flat fields, were taken to determine the scattering of light from the fiducial patches as a function of the phase of the moon. The lunar phase function was determined by July 1999, so that the BS-only nights were dropped – except for observations of the full moon. Full moon observations are still taken to determine the role of the opposition effect (Flatté et al. 1991) in the lunar phase function (phases  $-15^\circ$  to  $+15^\circ$ ). Current earthshine observations cover about 14 days per month, and cover lunar phases between  $\pm 40^\circ$  to  $\pm 150^\circ$  centered on the first and last quarters of the moon when we have optimal conditions for measuring the earthshine – close to full-earth with a few hours of observations being possible. Data rates vary depending on phase. An average night will give about 1 image per minute. This means that the number of raw images saved for data reduction, varies between 100 to 600 per night.

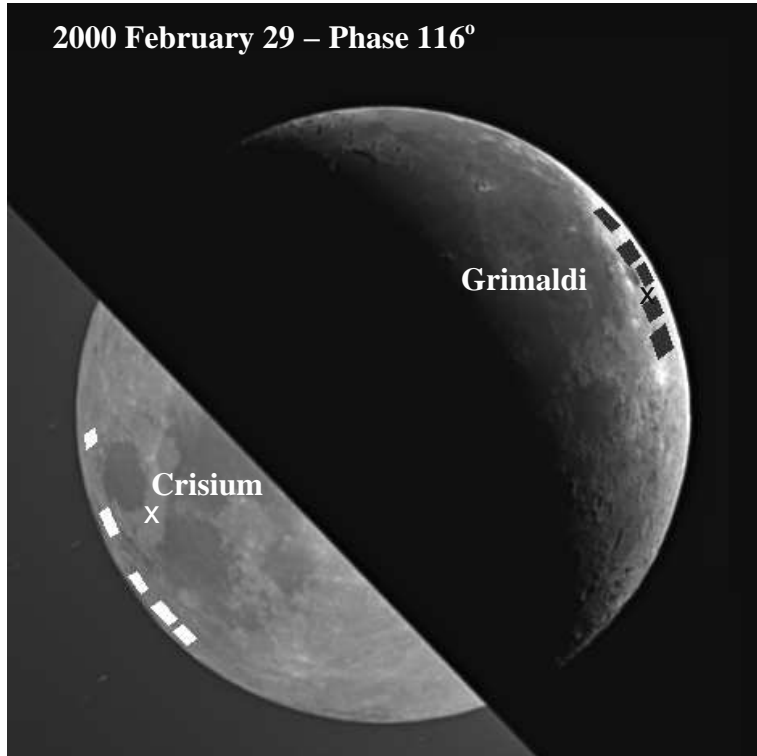


Fig. 3.— The moon showing the bright side and the earthshine. The Grimaldi side is in the moonshine and the Crisium side is in the earthshine. Our ten fiducial patches used in the observations made from BBSO are indicated. The crosses give the approximate positions of Danjon’s fiducial patches. Goode et al. (2001) used one fiducial patch on each side, and on the Crisium side it is the one closest to the white cross, while on the Grimaldi side, it is the one immediately above the black cross. In the image, the lunar phase is  $115^{\circ}.9$ , near a declining quarter moon. Unlike the moonshine, the earthshine is flat across the disk. The flatness is due to the uniform, incoherent back-scattering (non-Lambertian).

## 4. Data Reduction

### 4.1. Image Analysis

The earthshine and moonshine intensities are measured by integrating the brightness of a pair of fiducial patches – one from the bright side and the other from the dark side of the lunar disk. In our study, ten physically fixed fiducial patches have been used with five in the earthshine and five in the moonshine, see Figure 3. In selenographic (lunar) coordinates, the center latitudes and longitudes of the five patches on the Crisium side are (-17.5, -70.), (-11.2, -71.5), (-5., -76.), (0., -75.), and (7.5, -76.5), and those of the five patches on the Grimaldi side are (28.5, 72.5), (12.5, 75), (0., 77.), (-7.5, 75.), and (-13., 75.). Each patch covers a longitudinal range of about 10 degrees and latitudinal range of 3 to 5 degrees, the surface area being about 0.1% of the lunar surface, which corresponds to about 100 camera pixels. These patches are located in the “highlands” of the lunar surface, and the physical reflectivity of each is roughly comparable. One of the patches on the Grimaldi side is very close to Danjon’s choice, while the patches on the Crisium side are all closer to the limb than Danjon’s patch (Figure 3).

To locate these patches in each lunar disk image taken every night, it is essential to establish the transformation between the CCD image coordinate system and the selenographic coordinate system. For this purpose, we first define the limb and center of the lunar disk for each image. Each of the raw lunar images is contrast-enhanced, and the limb points are defined by looking for suitable positions of large intensity gradient. Empirically, a minimum of 40 rim points need to be obtained, and are then used to make a fitting to decide the lunar center in the image plane. Once the lunar center and limb are determined, the radius of the lunar disk is calculated in the CCD’s coordinate frame. The next step is to define the position of the lunar pole in the image plane. To this end, some outstanding lunar features, whose precise selenographic coordinates are known, are used to co-register the two coordinate systems. The topocentric location of the lunar pole at any given moment can be precisely calculated using parameters from an astronomical almanac, from which one can determine the projected positions of these lunar features in the image plane,



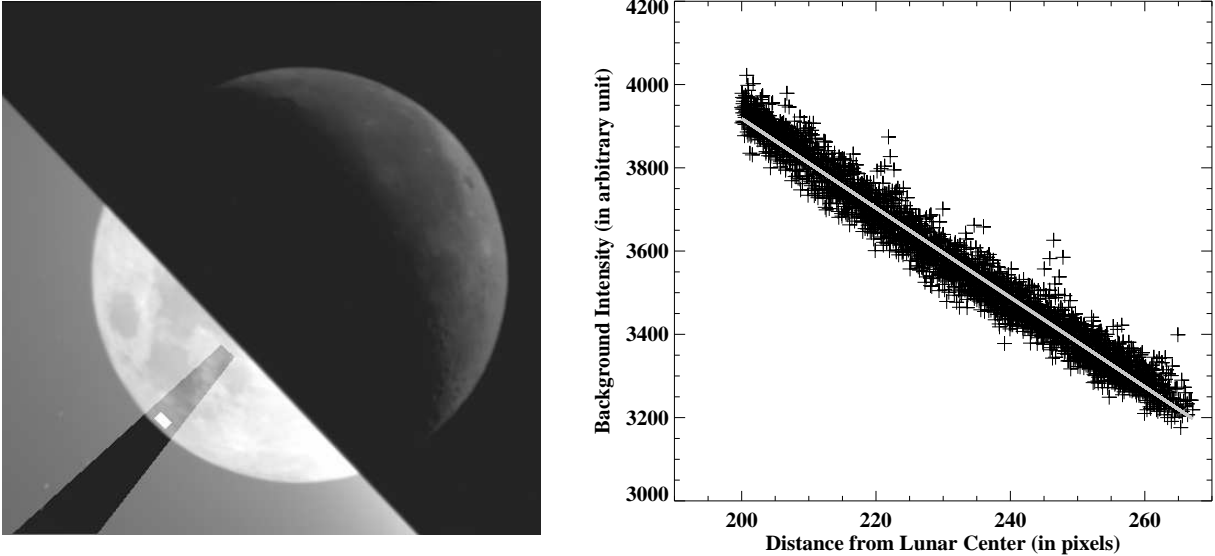


Fig. 4.— Illustration of the background subtraction for earthshine images. The image on the left shows a background cone around a fiducial patch, within which the intensity of the background points are read out to make a fit as a linear function of the distance from the lunar center. For the image shown, the intensity inside the cone has the background subtracted already. The plot on the right shows the decline of the off-limb intensity as the background point gets further from the lunar center, and the overplotted thick grey line indicates the least-square linear fit.

which is perpendicular to the vector pointing from the local observer to the lunar center. By comparing these projected positions with the positions of these features in CCD coordinates, the angle between the projected N-S axis of the moon and the Y-axis of the CCD coordinate system is derived.

Once the transformation between the image plane and the selenographic system is established, the five pairs of fiducial patches can be precisely located on the lunar disk image. The apparent areas of these patches change from night to night because of lunar libration. The intensity is read out as an average of the whole area, and the difference due to the geometric effect of the reflectivity arising from libration, is accounted for in our next step of data reduction (§4.2).

To ensure accurate photometry, flatfielding and dark current subtraction are performed on each image. For earthshine images, we also need to subtract the background scattering from the bright side of the moon. The background scattering should be a function of both the inclination of the vector connecting the lunar center and the background point with respect to the lunar equator, and the distance from the background point to the crescent. After experimentation, we found that we could safely assume that on the earthshine side, where the background points are not too close to the crescent, at a fixed inclination with respect to the lunar equator, the background intensity falls off linearly with the distance of the background point to the lunar center. Such a linear relation holds for the points which are not too far from the lunar equator. So, for each fiducial patch centered on the vector connecting the lunar center and the patch, we open a small cone with an angular size  $5^\circ$ , and fit the intensities of the background points, which are beyond the lunar limb and inside the cone, as a function of their distance to the lunar center. In this way, we can extrapolate the scattering intensity to the position of the fiducial patch using the parameters obtained from the least-square fit, and then subtract the linearly extrapolated value from the intensity of the fiducial patch. This procedure is illustrated in Figure 4.

In accordance with Equation (17), the intensity obtained from above is also corrected by scaling to a set of standard distances between the sun, moon and earth, before the successive steps of calibration described in subsequent subsections. Precise distance parameters are obtained from an ephemeris.

## 4.2. Atmospheric Extinction

To eliminate the effect of the atmospheric extinction, observations are carried out for as long as possible during the night so that a measurement of the intensity at varying airmass can be obtained. For the bright side of the moon, we expect the variation of the intensity to follow Beer's law:

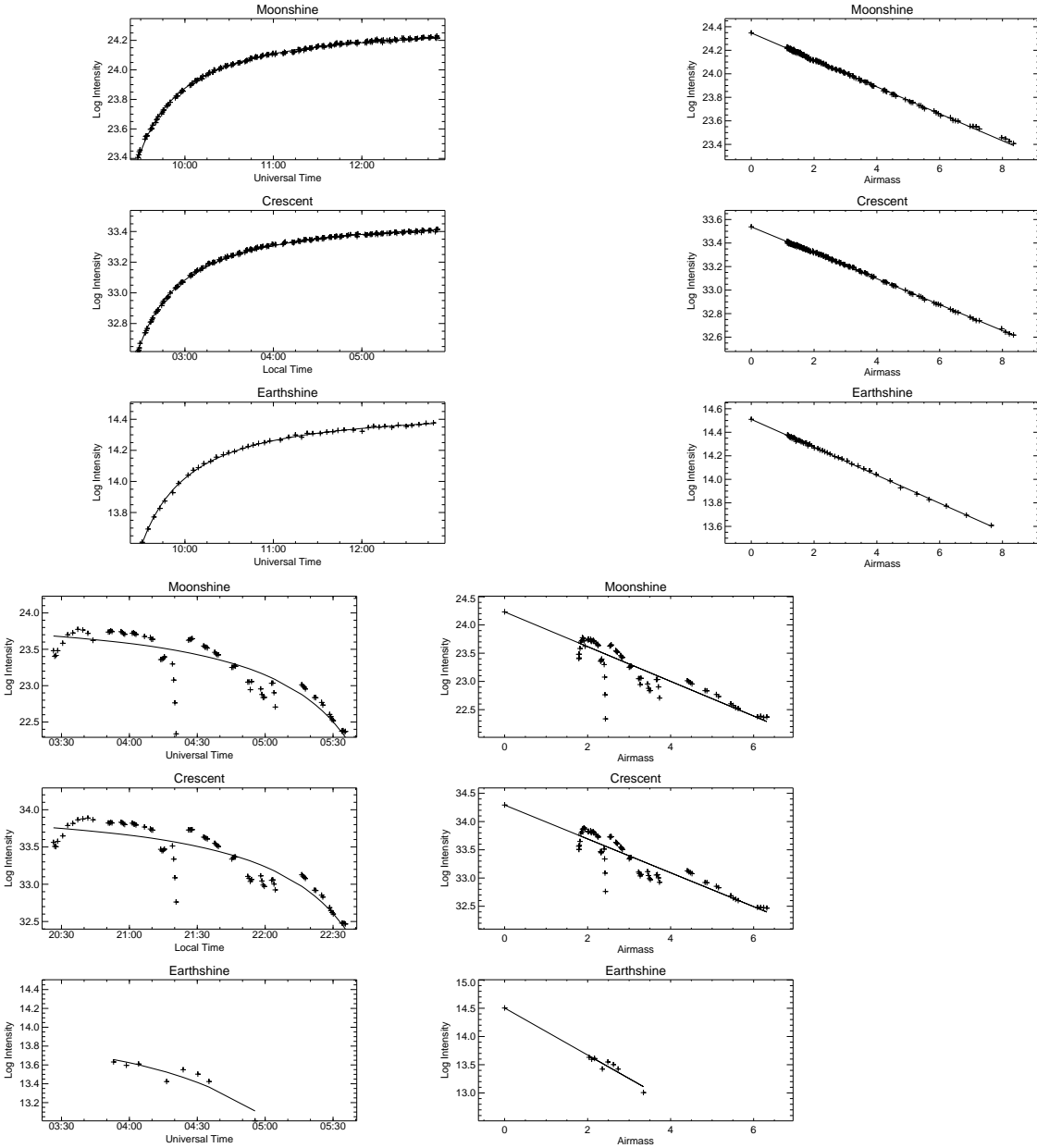


Fig. 5.— Each panel indicates either the moonshine (top panel of each triptych), the crescent (middle panel of each triptych), or the earthshine (bottom panel of each triptych) intensity plotted against time (on the left) and airmass (on the right). The “+” indicates observed data points and the solid lines are the fits to Beer’s law. Upper six panels: data from the night of September 5, 1999, demonstrating a typical good night, and the standard deviation of the fitting is 0.007, 0.005, 0.007 (from top to bottom). Lower six: data from the night of September 17, 1999, demonstrating a typical, partly cloudy night, and the standard deviation of the fitting is 0.219, 0.183, 0.077 (from top to bottom).

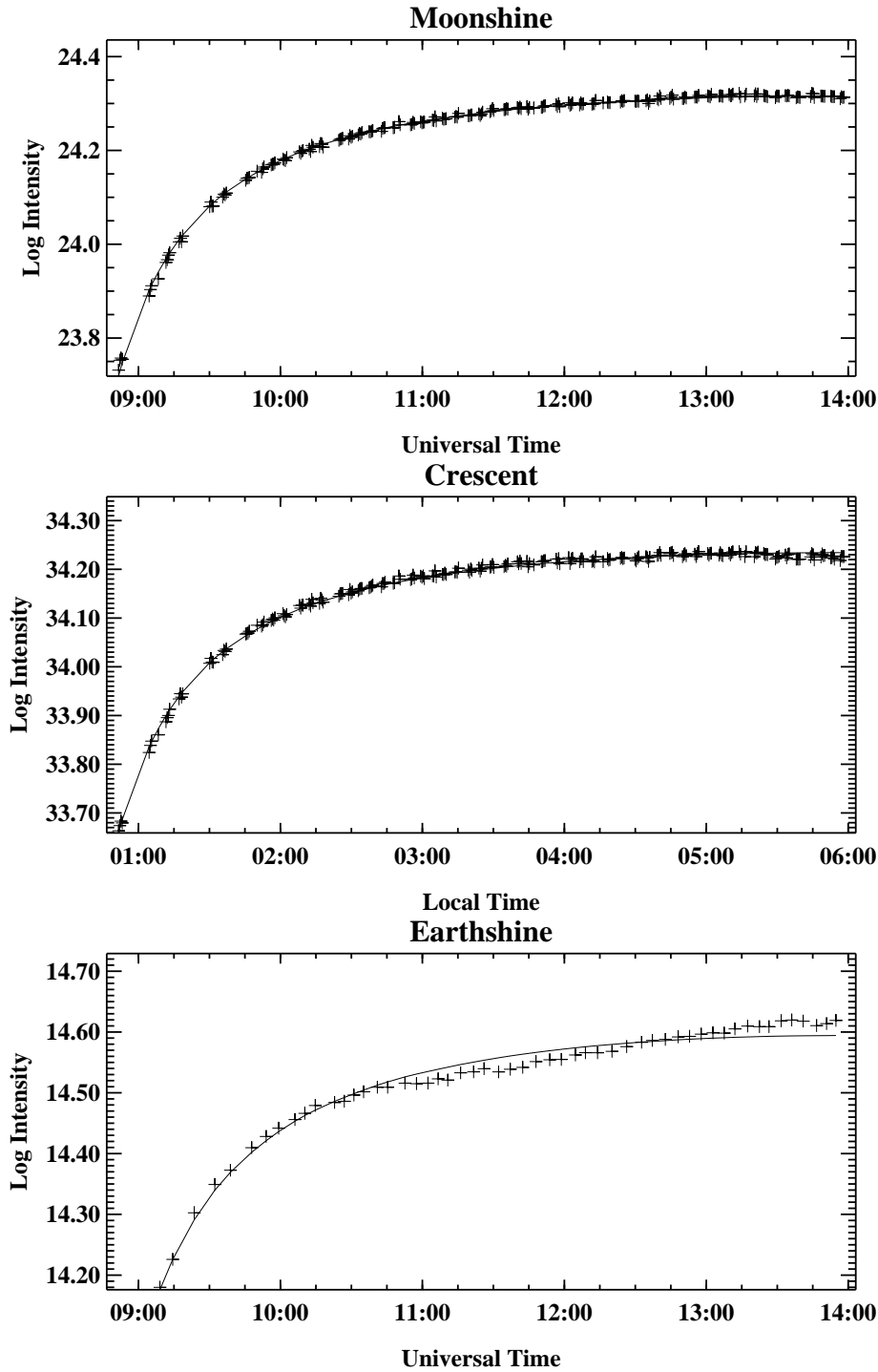


Fig. 6.— The moonshine, crescent and earthshine intensities and their Beer’s law fit for the night of 2000 January 28, showing that while the moonshine and crescent intensity follows Beer’s law very well, the earthshine intensity evolution deviates from Beer’s law. The standard deviations of the fits are 0.004, 0.005, 0.014, respectively. The fact that the fit is only poor for the earthshine implies sizeable short-term variations in the earth’s reflectance.

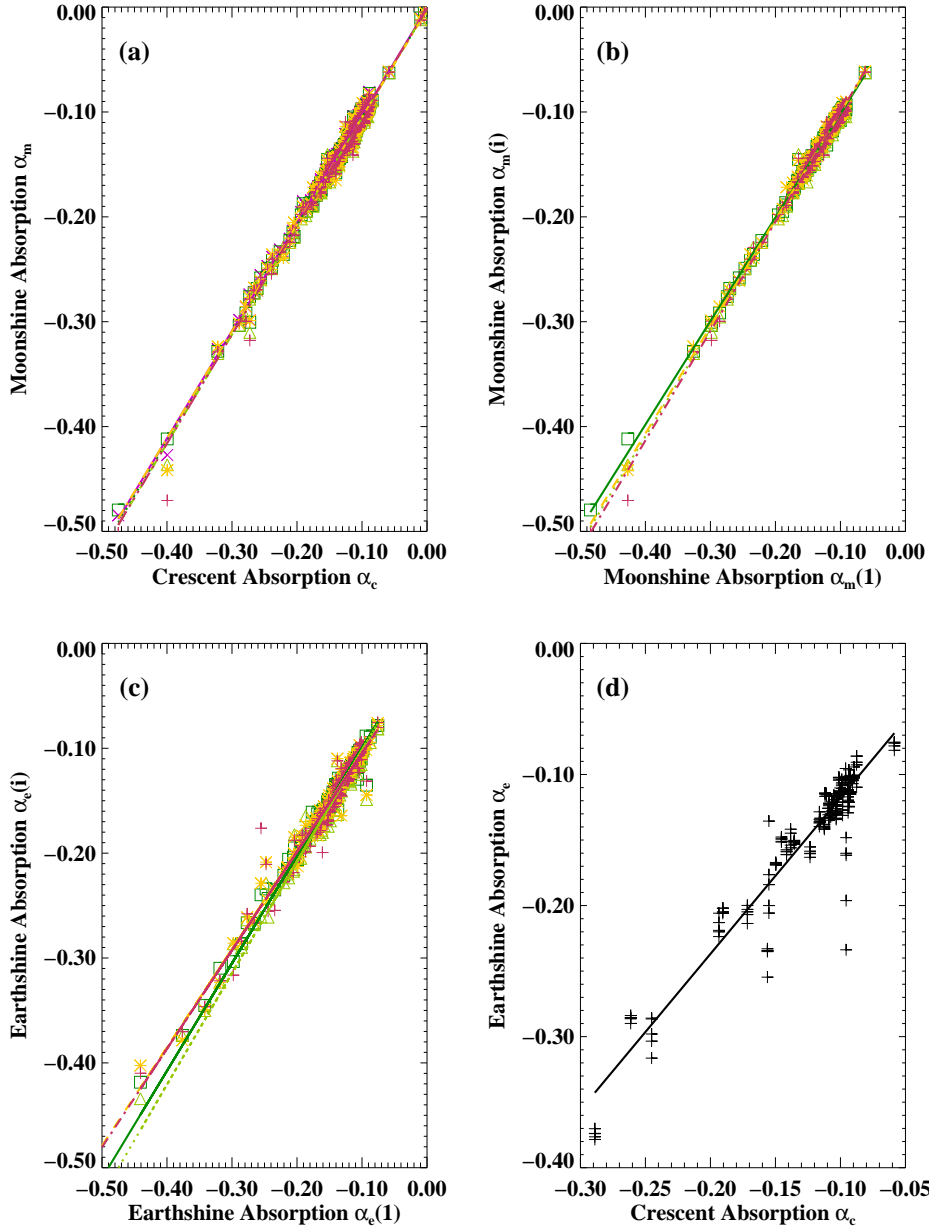


Fig. 7.— The variation of the atmospheric extinction coefficients for the crescent, ( $\alpha_c$ ), moonshine ( $\alpha_m$ ) and earthshine ( $\alpha_e$ ). Panel (a) illustrates  $\alpha_m$  (for five fiducial patches as indicated by different symbols) against  $\alpha_c$ ; (b) shows  $\alpha_m$  of four out of five fiducial patches (as indicated by different symbols) vs. the fifth fiducial patch, illustrating that  $\alpha_m$  is virtually the same for different patches (note the equivalence of each linear, least squares fits to the data for each patch); (c) shows  $\alpha_e$  for four out of five fiducial patches (as indicated by different symbols) vs. the other fiducial patch, showing that  $\alpha_e$  is also the same for different fiducial patches in the earthshine; and (d) shows  $\alpha_e$  (of all fiducial patches in earthshine) against  $\alpha_c$ . The various straight lines in each panel indicates a least squares fit to the appropriate data.

$$I = I_0 e^{(-\alpha z)}, \tag{18}$$

where  $I$  is the observed intensity,  $\alpha$  is the atmospheric extinction coefficient,  $z$  is the local airmass and  $I_0$  is the intensity at zero airmass – the intensity if the earth had no atmosphere.

The airmass,  $z$ , is determined from the angular altitude of the moon in the sky at different times in such a way that when the co-latitude  $\theta_c$  - the inclination of the observer’s line of sight with respect to the local zenith, which is the complement of the moon’s angular altitude - is smaller than  $60^\circ$ ,  $z = 1./\cos(\theta_c)$ ; otherwise  $z$  is interpolated from a standard airmass table (Table 1):

The above calculation refers to the airmass at sea level with the pressure  $p_0 = 760$  mmHg and temperature  $t_0 = 10^\circ C$ , and the real airmass at the observer’s location must be corrected by a multiplicative factor of  $p/p_0/(0.962 + 0.0038t)$  (C. W. Allen, 1973, *Astrophysical Quantities*, p.125). BBSO is 2067m above sea level, and the pressure scale height at this altitude is 8200m, which yields  $p = p_0 \exp(-2067./8200.)$ . We then incorporate the calculated  $z$  into the Beer’s law fitting to determine  $\alpha$  and  $I_0$ . We reckon that throughout a night, the evolving lunar phase function can also contribute to the changing intensity. The maximum phase change in a long night is less than two degrees, within which the intensity change is negligible compared to the change due to the airmass. Nevertheless, we employ a quasi-iterative way to correct this minor effect, in that we use an initial fit of the phase function (see the following section on how to obtain the phase function) to correct the data, and after the airmass correction, we make the phase function

Table 1: Standard Airmass Table ( $\theta_c$  in degrees)

$\theta_c$	60.	62.	64.	66.	68.	70.	72.	74.	76.	78.	80.
$z$	2.00	2.12	2.27	2.45	2.65	2.90	3.21	3.59	4.07	4.72	5.60
$\theta_c$	81.	82.	83.	84.	85.	86.	87.	88.	89.	90.	-
$z$	6.18	6.88	7.77	8.90	10.39	12.44	15.36	19.79	26.96	40.00	-

fit again. After a few iterations, the data converge to a stable result. The observed intensity at each moment,  $I_i$ , is corrected, using the airmass, to the intensity at zero airmass,  $I_i^0 = I_i \exp(\alpha z)$ .  $I_0$  from the fitting is further used as the intensity for that night’s lunar phase function.

The goodness of the fit to Beer’s law offers a ready criterion by which each night’s local sky can be judged – the “good” night’s data can be separated from that of the “bad” (noisy) night’s (Figure 5). In practice, unless it is cloudy the data from almost all observable nights are preserved, and the standard error in the fitting for each night is further used as the input error for the lunar phase function fit. Figure 5 shows an example of a typical good night and a bad night, as judged by fitting to Beer’s law. Experience from the observations shows that the data usually follow Beer’s law quite well, and the accuracy of the moonshine fitting is often better than 1%. Among all the datasets collected for 340 nights from November 28, 1998 to March 31, 2002, the accuracy of the fitting is better than 1% for 110 nights, and the accuracy is between 1% and 2% for 139 nights, and between 2% and 3% for 52 nights.

In the case of earthshine intensity, apart from the atmospheric transmission, the evolution of the earthshine is also influenced by changing of the earth during a given night; e.g., the sun rising over a cloudy China. In addition, almost every month, on a few nights, we observe that the evolution pattern of the earthshine intensity does not track Beer’s law in an unambiguous way, even though the moonshine intensity closely follows Beer’s law. An example of such a case is shown in Figure 6. In general, the fit to the earthshine yields a standard deviation that is larger than that for the moonshine fitting by one-half to one percent. This latter difference contains the signal of the earth’s albedo. On such nights when the evolution of the earthshine is significantly controlled by real changes in the earth’s reflectance, apart from the atmospheric extinction, as illustrated Figure 6c, the atmospheric absorption coefficient  $\alpha$  obtained from the Beer’s law fitting of the earthshine observations may deviate from the true value. That is, some part of the earthshine signal may be subsumed into the atmospheric extinction, and vice versa, so that the correct atmospheric attenuation cannot be properly determined from the standard Beer’s law fitting.

To deal with this problem, we investigated the relationship between the earthshine coefficients,  $\alpha_e$ , and the moonshine coefficients,  $\alpha_m$ . As a reference, we have also examined  $\alpha_m$  for different  $\alpha_e$ , and the moonshine coefficients,  $\alpha_m$ ; we have also examined  $\alpha_m$  for different fiducial patches and  $\alpha_c$ , the fitting parameter for the integral intensity of the whole crescent. Figure 7 (a) and (b) show the relationship between  $\alpha_c$  and the  $\alpha_m^i (i = 1, 2, 3, 4, 5)$  for all five fiducial patches. Least-square fits reveal that the  $\alpha_m^i (i = 1, 2, 3, 4, 5)$  can be regarded as being identical to one another, and to  $\alpha_c$ . This is not a surprise even though, as it is well known, the atmospheric attenuation is also a function of the wavelength, as the light from a moonshine fiducial patch should have the same spectrum as the light from the whole bright side. Similarly, the earthshine absorption coefficient,  $\alpha_e$ , is linearly correlated with  $\alpha_c$  (Figure 7 (d)), but the absolute value of  $\alpha_e$  is systematically larger than that of  $\alpha_c$ , indicating a stronger atmospheric attenuation in earthshine than in moonshine. This is because the earthshine and the moonshine have different spectra; specifically, the earthshine is bluer than the moonshine because the bluer the light the more effectively the earth’s atmosphere scatters it away.

The solution to fitting nights like those shown in Figure 6 lies in exploiting the linear scaling law that we find between  $\alpha_e$  and  $\alpha_c$ , which enables us to make a better determination of  $\alpha_e$  from  $\alpha_c$  for the nights when the usual, local airmass changes leading to a good Beer’s law fit for the moonshine are compounded by sharp earthshine variations such that the mixture yields observational data that deviates sufficiently from Beer’s law, so that one cannot be confident of the fit obtained in the usual way. Our solution lies in using  $\alpha_c$  to fix  $\alpha_e$  for the problematic nights, beginning with

$$\alpha_e = a \times \alpha_c + b, \tag{19}$$

where the scaling parameters  $a$  and  $b$  are obtained by a linear least-square fit of the above relation using  $\alpha_e$  and  $\alpha_c$  from the nights that do not show apparent global evolution that strays strongly from the Beer’s law fit. We reckon that for the nights of significant global change, the standard deviation of the Beer’s law fitting of the earthshine ( $\sigma_e$ ) must be a lot larger than that of the crescent ( $\sigma_c$ ), given that the local atmosphere is reasonably stable throughout a single night. For



Table 2:  $\alpha_e$  against  $\alpha_c$

q	a	b	$\sigma$	$\sigma_a$	$\sigma_b$
1.0	1.1886	-0.0073	0.0099	0.0183	0.0023
1.2	1.1830	-0.0061	0.0128	0.0170	0.0023
1.5	1.1813	-0.0051	0.0132	0.0172	0.0023
1.8	1.1881	-0.0050	0.0140	0.0171	0.0023
2.0	1.2281	-0.0095	0.0167	0.0169	0.0023
2.5	1.2222	-0.0124	0.0164	0.0161	0.0022

this reason, we make a further assumption that when  $\sigma_e$  is less than a cutoff value  $q$  times  $\sigma_c$ , i.e.,  $\sigma_e < q\sigma_c$ , we regard the global change as not being significant during this night, and  $\alpha_e$  from the Beer’s fitting for this night is reliable. Only then do we use these nights to make the fit in order to determine  $a$  and  $b$ .

In Table 2, we list the fitting results,  $a$ ,  $b$ ,  $\sigma$  (the standard deviation of the fit),  $\sigma_a$  and  $\sigma_b$  (the fitting errors of  $a$  and  $b$  respectively) for various cutoff values,  $q = 1.0, 1.2, 1.5, 2.0, 2.5$ .

We can see from Table 2 that for  $q < 2.0$ , the fitting results are consistent with each other. In general, the absolute value of  $\alpha_e$  is larger than that of  $\alpha_c$  by more than 0.01, or about 10%. That is, using  $\alpha_c \sim 0.1$  and Table 2, we have  $\alpha_e \sim 1.2 \times \alpha_c - 0.01 \sim 0.11$ . Note that we do not distinguish among the  $\alpha_e$  from different fiducial patches, because there is no reason for us to believe that the  $\alpha_e^i$  should be different from one another (also see Figure 7c). As a matter of fact, we have tried to scale  $\alpha_e^i$  to  $\alpha_c$  separately, and the resulting fitting parameters  $a$  and  $b$  do not differ for different patches. In the subsequent analysis, we employ the scaling parameters at  $q = 1.2$  in Equation (19) to obtain  $\alpha_e$  from  $\alpha_c$  for nights when  $\sigma_e > 1.2\sigma_c$ . Then, we use  $\alpha_e$  to fit out the atmospheric attenuation, so that we can determine the true earthshine signal. After applying this correction, a direct result is that while the average of the [A\*] is not altered, for some nights their appreciable, original deviations from the average, at comparable lunar phase, is greatly reduced.

For those same nights the calculated  $\alpha_e$  yields a slightly poorer fit to the data than would a direct fitting to Beer’s law. The price of this latter fitting was to force some of the earthshine signal into the atmospheric extinction coefficient, yielding an erroneous extrapolation to zero airmass.

### 4.3. Measuring the Transmission of the Bright Side Filter

A precise determination of the earth’s reflectance from observing the moon depends on an accurate measurement of the ratio of the true earthshine intensity to the true moonshine intensity. This determination is complicated by the fact that the moonshine is so bright that when we measure it, we must use a filter (see Figure 3) that reduces the intensity of the moonshine by about 99%. The reduction enables us to have a reasonably long exposure time (of order a few 100 ms) compared to the shortest possible exposure time of the camera (10 ms). When we observe the earthshine, the moonshine or BS filter flips out and the much stronger, blocking filter flips in to block the moonshine to prevent camera blooming during the much longer exposures. Thus, to know the true ratio of the earthshine to moonshine intensity, we must also precisely determine the transmission of the moonshine filter at the point through which the moonlight passes. This fact became abundantly clear after October 13, 2000 when the original filter was destroyed, and was replaced by one that was comparable in the lab specifications for the transmission over the whole filter. Initially, we assumed that the transmission of the new filter was the same as the old one. However, we found that the observed moonshine intensity noticeably increased indicating that the new filter has a significantly larger transmission than the old filter.

In the observations, the moonshine filter, MS, is placed at a fixed position in the focal plane covering the entire lunar image, so that the light always passes through the same point on the filter. This is important because there is some point-to-point variation in the transmission of the filter. In our effort to precisely determine the transmissions of the old and new BS filters at the focal point of the lunar image, we first employed identical approaches for both of the filters. To measure the transmission of the old filter, we re-analyzed thirty nights of moonshine and earthshine data that we had in-hand for nights near the new moon - where the earthshine signal is most intense.

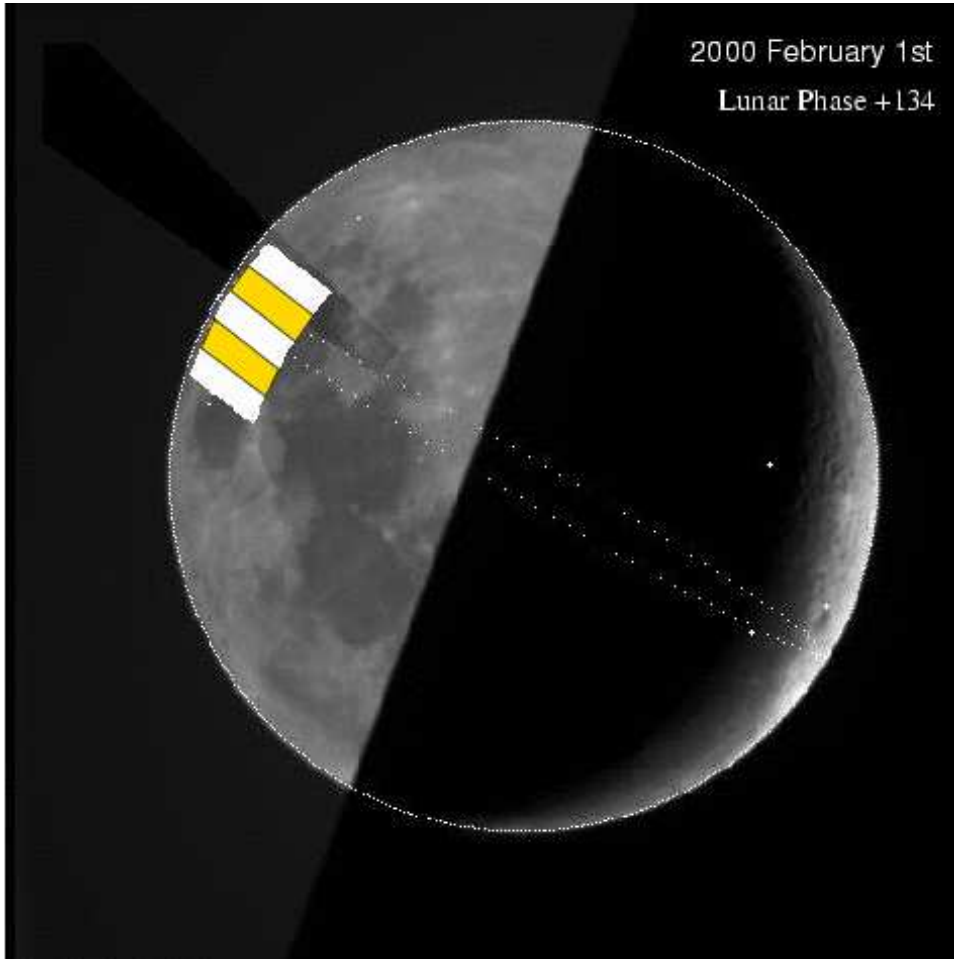


Fig. 8.— Image of the earthshine on the night of February 1, 2000 shown is one with the blocking filter, which enables long exposures of the earthshine. The bright, rectangular patch indicates the area of five strips used to compare the earthshine intensity with and without the moonshine filter (BS filter), so as to determine the transmission of the BS filter. The lunar phase was  $+134^\circ$  that night, and so the earthshine signal is relatively strong. The crescent is not visible through the strong blocking filter in the original image, but has been restored here for reference.

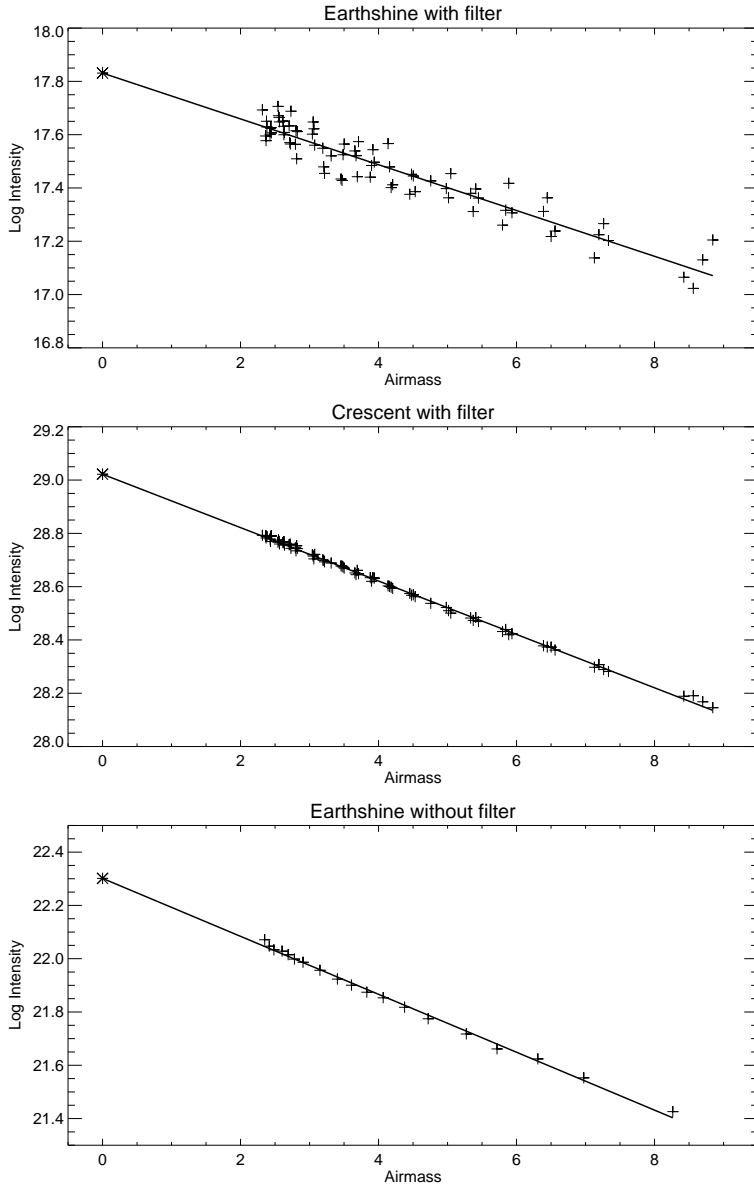


Fig. 9.— The upper panel shows the observed, BS filter-blocked earthshine intensity as a function of airmass on February 1, 2000. The “+” signs in that panel represent the intensity of one of the stripes. The linear fit to the data has been extrapolated to zero airmass with that result being indicated by the asterisk, which is the left-most mark on the fit. The lower panel shows the same type of data, but without the BS filter. The ratio of the two intensities, for that night, extrapolated to zero airmass, and corrected for the small effect of stray light, implies a MS filter transmission of  $0.0114 \pm 0.0005$ . The lunar phase that night was  $+134^\circ$ .

To illustrate the re-analysis procedure, one can look at Figure 8 for guidance. For that night, with the old filter, we measured the total earthshine intensity in five parallel strips, somewhat wider than the fiducial patches and running from the earthshine fiducial points toward the moonshine crescent. In that figure, the five strips are shown together as a striped, bright four-cornered patch. Each strip in the bright patch runs from the edge of the moon and is  $5^\circ$  wide in latitude and  $30^\circ$  long in longitude. That way, each strip would have a statistically significant number of counts in the earthshine region, even for the relatively short exposure times of a few hundred milliseconds, used on that, and other nights, for each data point with the BS filter in place (but without the much stronger blocking filter in place). The lunar phase in Figure 8 is  $+134^\circ$ . Large magnitude phase angles are chosen so that the earthshine is the brightest, while the stray light the smallest. The determination of the transmission of the old BS filter is shown for that typical night in Figure 9. The dark side of the moonshine and the earthshine intensities are each extrapolated to zero airmass, and corrected for the small effect of stray light, (as described in §4.1), and their ratio yields a transmission of  $0.0114 \pm 0.005$  for that night. The error weighted mean transmission for all thirty nights is  $0.01127 \pm 0.00011$  for the old filter. Implicit in this approach to determining the broadband transmission of the filter is the assumption that the spectrum of the earthshine and moonshine are roughly the same; this assumption works here because the transmission curve is flat over visible wavelengths. Most of the noise in the result arises from the short exposure time for the MS filter covered observations. The  $0.01127 \pm 0.00011$  is within the factory quoted errors of the 0.0115 value given by Schott.

For the new filter, we have re-analyzed twelve nights of data in the same way and find a transmission of  $0.01338 \pm 0.00017$  for the focal point, whereas the factory reported the average across the filter is 0.0114. The latter transmission is nearly identical to that of the old filter, but quite far from  $0.01338 \pm 0.00017$ . The larger transmission at the focal point accounts for the apparent rise in moonshine intensity after October 13, 2000. We will continue collecting more data on the transmission using future data. However, we have a more powerful and more precise cross-check in hand – using lunar phase function data on the crescent and moonshine, which we know to 0.5%.

Analyzing all of our good nights of moonshine observations, with the new and old new filter, at all phases, we have constructed for each a lunar phase function – the change in brightness with lunar phase for the moonshine and crescent intensities. From all these nights, we have selected the nights during the period for which the old filter was used, and then we calculated a second-degree polynomial fit to the lunar phase data. The data for these nights have been reduced using a transmission value of 0.01127. After that, we analyze the phase function for the nights taken with the new filter and calculate the standard deviation of the values to the lunar phase function fit to the old data, but leave the new filter transmission as a variable.

Our procedures consist of multiplying the intensities of the new phase function data by a factor between 0.9 to 1.4 in steps of 0.0001, and for each case calculating the standard deviation to the old data fit. The agreement of the new data with the fit to the old data will be optimal when the standard deviation is minimized.

We find the best agreement between the two lunar phase functions when the transmission of the new filter is 0.0132 (0.01319 for the moonshine and 0.01322 for the crescent). This is excellent agreement with the transmission determined from the first method. Thus, we have precisely determined the transmission of the new filter to the same precision as the old filter, so that we use  $0.0132 \pm 0.0001$  as its transmission after including errors in the phase function. As we gather more data on the new filter, we can determine its transmission to the same precision to which we know the lunar phase function, and then the error on the transmission can be reduced to about  $\pm 0.00005$ . Following that, we can use this information to reduce the quoted precision of the old filter to that for the lunar phase function determined for the old filter.

## 5. The Lunar Phase Function

The lunar phase function is defined as the normalized change in the moonshine intensity as a function of lunar phase, which represents the geometric reflectance of the moon. It is measured from the readout intensity of each of the fixed fiducial patches (five on the Crisium side and five

on the Grimaldi side) used throughout the observations, after carrying out several straightforward corrections to the raw scattering data. When the raw, observed intensity readout is plotted against the lunar phase for all nights, the data are quite scattered around a different means for each branch, as illustrated in Figure 10 for the Crisium and Grimaldi pair used in Goode et al. (2001). This figure, and that pair, are treated in detail in this section. The raw results for all pairs take the same form as the chosen pair. On the face of it, the large scattering in Figure 10 would seem to preclude a precise determination of the earth’s albedo from measuring the earthshine. However, most of the scattering is due to known physical effects for which one can systematically account, and then remove.

The first factor is the night-to-night change of the local atmosphere, apart from the nightly atmosphere attenuation which follows Beer’s law. Such a change affects the measured crescent as a whole, and moonshine and earthshine from the fiducial patches in precisely the same way, and hence, the raw phase function by can be corrected by treating the crescent as a standard star (see §5.1). This correction does not alter the determination of  $A^*$ , because the correction applies to both the earthshine and moonshine, while  $A^*$  is given by the ratio of the earthshine to the moonshine. The second factor is the sun’s position, namely the declination and right ascension, due to the changing angle of the sunlight into the earth-moon system at the same lunar phase, but in different synodic months. To first order, we fit out the alteration of the scattering introduced into the phase function. (see §5.2). Since it affects the moonshine and earthshine intensities in the same way, again  $A^*$  is insensitive to the change. The third known source of the scatter in Figure 10 is the moon’s libration, which changes the observed intensity from the moonshine fiducial patches, but does not affect the earthshine intensity (see Figure 3 in which the non-uniformity of the moonshine near the limb is apparent, but there is no such non-uniformity in the earthshine). To first order, we model this effect as a linear function of the libration and correct it for both the phase function and in the moonshine intensity  $I_b$ , when using  $I_b$  to calculate  $A^*$  (see §5.3). The results of these corrections are developed in this section, one step at a time. We shall see that we can determine the lunar phase function to 0.5%, which gives us real confidence that observing the earthshine can yield a precise reflectance for the earth.

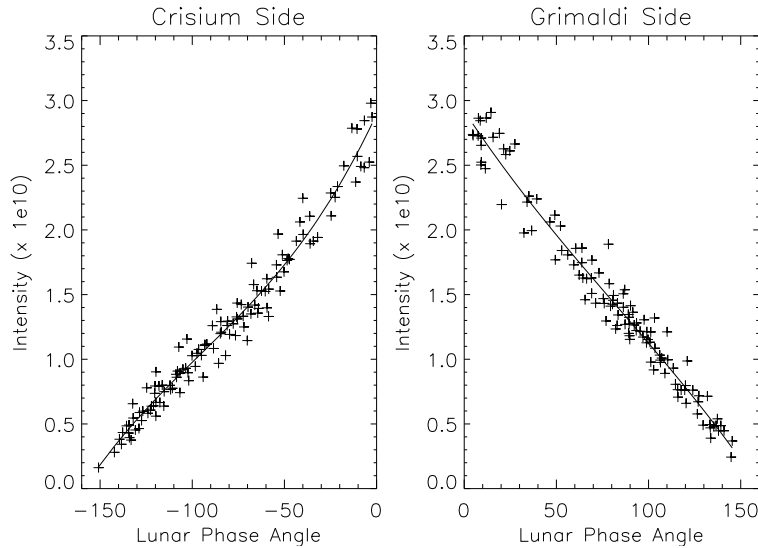


Fig. 10.— The intensity of the *moonshine* for the Crisium side and Grimaldi side fiducial patches of Goode et al. (2001) with a third order polynomial (including higher order terms has no noticeable effect) fit for each. Clearly, there is a roughly linear decrease in the intensity of the reflected light going from full moon to new moon.

In the last part of this section (§5.4), we normalize the overall lunar phase function to connect the right and left branches of the lunar phase function by treating the opposition surge that occurs at small phase angles. The data here are from the fullest of full moons and the one total lunar eclipse we observed in Big Bear. The total eclipse enables us to determine the ratio of the geometrical albedos of the opposing pairs of fiducial patches.

### 5.1. Atmospheric Correction

The nightly fits of the moonshine intensity to Beer’s law are quite good, and so the extrapolation to zero airmass would seem quite reliable. However, there is an appreciable change in our lunar phase function (see Figure 10), for the same phase, from month-to-month. As we shall see, the prime cause of this is that, even after extrapolation to zero airmass, the resultant intensity is subject to changes in the local atmospheric conditions. It seems that the local atmosphere is not



a uniform plane, parallel gas, but rather we have something more like a canopy superposed on a plane parallel atmosphere. The canopy mutes the intensity by the same amount for all airmasses, and therefore its effect remains after extrapolation. Because of this, there is a deviation in the intensity measured from the same fiducial patch at the same lunar phase, but on different nights (that is, successive lunar cycles). To solve this problem, we employed the common practice of nighttime observers doing absolute photometry who use standard stars to account for the muting. We have found that the crescent of the moon is our best standard “star”. That is, we correct from night-to-night variations using the correlation between the change of the moonshine intensity and the crescent intensity.

In the extrapolation to zero airmass, we use a fifth degree weighted polynomial fit for both the fiducial patch intensity and the average crescent intensity over the area of the bright portion as the way to determine the average of the intensity at each lunar phase. In removing the canopy effect, we give double weight to nights for which the lunar phase is less than  $\pm 5^\circ$ . We do this because of the pronounced opposition effect that gives a sharp increase in the moonshine intensity when lunar phase approaches zero degrees (see §5.4). The deviation of the measured intensity at each data point from the fitting curve for the lunar phase function, in both the moonshine case and the crescent case are obtained, and the cross correlation between these deviations is calculated. For the morning observations, for which the lunar phase is positive, we get a cross correlation of 0.73, and for the evening when the lunar phase is negative, we obtain a quite similar value of 0.77 (Figure 11). The relative correlations are determined from a simple least-square linear fit between the moonshine deviation and crescent deviation using

$$\frac{I_i - \bar{I}_i}{\bar{I}_i} = a_0 \times \frac{C_i - \bar{C}_i}{\bar{C}_i} + b_0 + \sigma_i, \quad (20)$$

where  $I_i$  is the observed fiducial patch intensity,  $C_i$  is the crescent intensity,  $\bar{I}_i$  and  $\bar{C}_i$  are the average fiducial patch intensity and crescent intensity, respectively, at the same lunar phase, and  $\sigma_i$  is the scatter about the linear least-squares fit. Note that throughout this section  $\bar{I}_i$  is the final, fitted intensity, which is derived by iterating the steps described in §5.1-5.3. The coefficients  $a_0$  and  $b_0$  are derived from the least square fitting of Equation (20). From Figure 11, it is clear

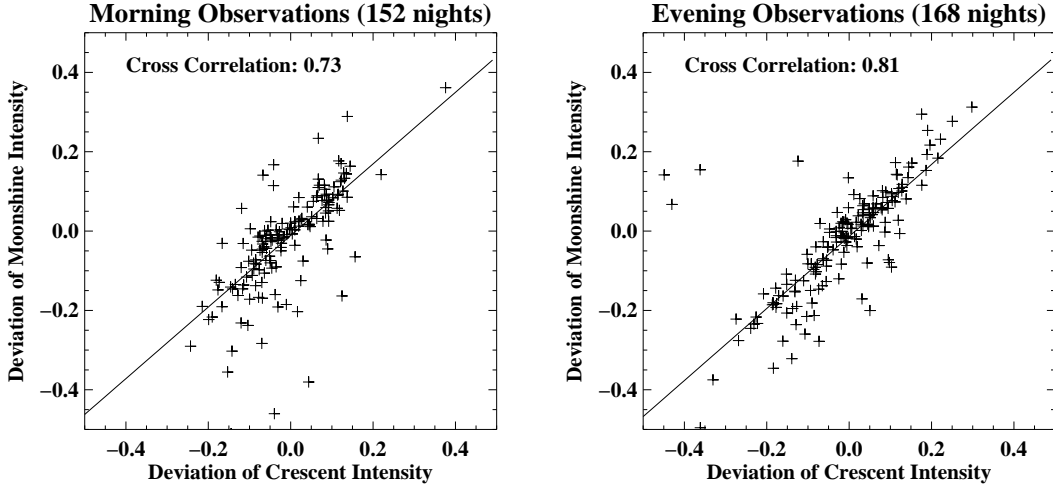


Fig. 11.— The deviation of the moonshine fiducial patch intensity from average against the deviation of the overall intensity of the crescent. Left: data points from morning observations of Grimaldi; right: data points from evening observations of Crisium. The solid lines in each panel show the linear fit to each cluster of points.

that  $a_0$  is close to unity (morning/Grimaldi:  $0.81 \pm 0.08$  and evening/Crisium:  $0.74 \pm 0.07$ ), while the respective  $b_0$ 's are essentially zero – 0.002 and 0.001 – more than two orders of magnitude smaller than  $a_0$ . Therefore, we determine the correct, relative zero airmass intensity,  $I'_i$ , by removing the canopy effect by subtracting the linear term in Equation (20) from the earthshine data, i.e.,

$$I'_i = I_i - a_0 \times \bar{I}_i \times \frac{C_i - \bar{C}_i}{C_i}. \quad (21)$$

The scattering among the datapoints is much reduced after this correction. This correction is of comparable significance for the evening data (lunar phase  $< 0$ ) and the morning data (lunar phase  $> 0$ ), as the comparable cross-correlations imply.

## 5.2. Declination Correction

The second step in correcting the deficiencies in the apparent lunar phase function is to remove variations arising from the systematic change of relative position of the moon to the plane

of the earth’s orbit about the sun. The difference in right ascension between the sun and the moon (hereafter, the “relative right ascension”) changes from 180 to  $-180^\circ$ , which essentially determines the lunar phase, defined as the angle from between the moon-earth line and the sun-moon line, see Figure 1. However, there is a clear ambiguity in the lunar phase angle that makes the apparent lunar phase function multi-valued. In detail, the difference in the declination between the sun and the moon (hereafter “relative declination”) changes as well, since the orbital plane of the moon around earth is inclined to that of the earth around the sun. Toward the full moon, the relative declination also becomes important in determining the lunar phase. Then, at the same lunar phase, but on different nights (that is, different months), the position of the moon may be different, and this difference alters the readout intensity of the fiducial patches. To correct for this effect, for a given lunar phase near the full moon, we choose a standard position of the moon and normalize the readout intensity of different positions to this standard position. The standard position is the one for which the relative declination is zero, i.e., the moon is in the plane of ecliptic, and the lunar phase is equal to the relative right ascension, i.e., a total lunar eclipse. The normalization is made as follows:

$$I_i - \bar{I}_i = a_1(P_i - P_{i,RA}) + b_1D_i + c_1 + \sigma_i, \quad (22)$$

where  $I_i$  is the observed intensity,  $\bar{I}_i$  is the average intensity at the same lunar phase as  $I_i$  (from the ultimately determined lunar phase function),  $(P_i - P_{i,RA})$  is the difference between the lunar phase and the relative right ascension,  $D_i$  is the relative declination, and  $a_1$ ,  $b_1$ , and  $c_1$  are fitting parameters, which are determined from the least square fitting using all the observed intensities. The fitted parameters,  $a_1$  (morning/Grimaldi:  $-0.003 \pm 0.002$  and evening/Crisium:  $3.4e-5 \pm 7.0e-5$ ),  $b_1$  (morning/Grimaldi:  $-0.4.7e-5 \pm 0.0002$  and evening/Crisium:  $0.0007 \pm 0.0002$ ) and  $c_1$  (morning/Grimaldi:  $0.009 \pm 0.008$  and evening/Crisium:  $0.009 \pm 0.009$ ) are all quite small. The normalized intensity,  $I'_i$ , is derived by removing the relative right ascension and declination:

$$I'_i = I_i - [a_1(P_i - P_{i,RA}) + b_1D_i]. \quad (23)$$

The  $c_1$  term is regarded as part of the errors ( $\sigma_i$ ).

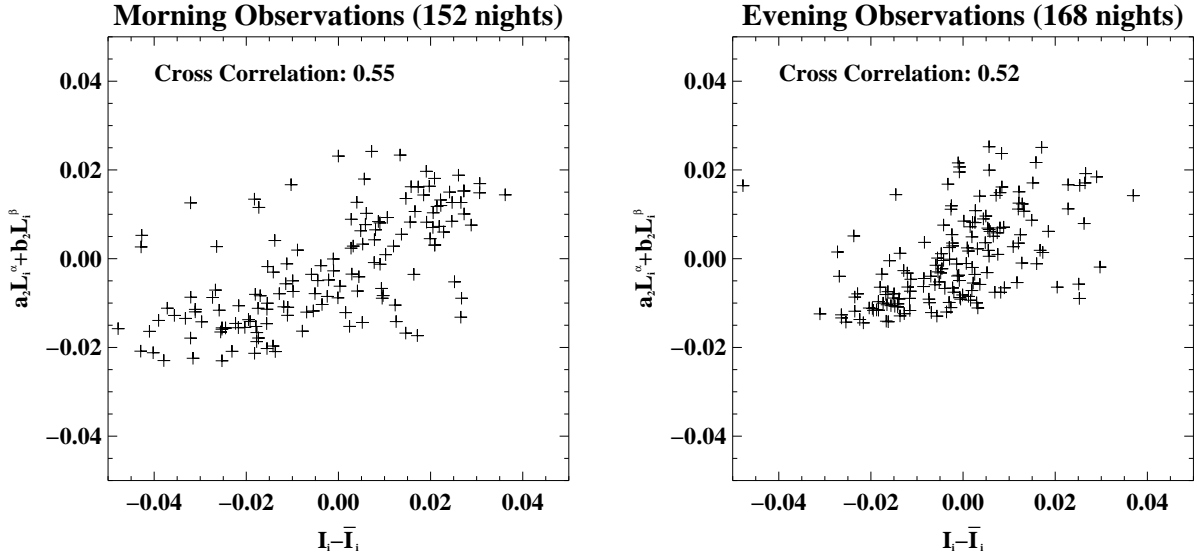


Fig. 12.— The deviation of the moonshine fiducial patch intensity (after the first and second step corrections) from average against the deviation as a fitting result from Equation (24). Left: data points from morning observations; right: data points from evening observations.

This correction is only made for lunar phase between  $-15$  and  $+15$  degree since the effect of the relative position of the moon is only important around the full moon. However, after this correction, the modest improvement reveals barely apparent changes in the data points.

### 5.3. Libration Correction

The third step in rectifying the apparent lunar phase function requires removing the effects of latitudinal and longitudinal lunar libration. Since the orbit of the moon around the earth is not in the equatorial plane of the moon, a terrestrial observer alternatively sees the north pole and south pole of the moon during each orbit. This is the latitudinal libration. Further, the slightly elliptical orbit of the moon has the consequence that the moon moves more slowly at apogee than at perigee, and therefore is seen to be wobbling around its axis of rotation. This is longitudinal libration. An additional, very small dynamical libration arises because the moon is prolate, and its pointing wanders. The dynamical libration adds to both the latitudinal and longitudinal

librations. These librations allow us to see about 60% of the moon’s surface. As a result of both kinds of libration, for different cycles of the lunar orbit, even at the same lunar phase, we would expect changes in the positions of the fiducial patches on the lunar disk. The readout intensity thus changes as a function of the geometric position of the fiducial patches on the lunar disk. The longitudinal and latitudinal librations cause the apparent lunar phase function to be multi-valued. To first order, we derived a description of the deviation of the observed intensity from the averaged intensity as a linear function of the longitudinal and latitudinal librations, which goes as:

$$I_i - \bar{I}_i = a_2 L_i^\alpha + b_2 L_i^\beta + c_2 + \sigma_i, \quad (24)$$

where the  $I_i - \bar{I}_i$  are the deviations of each night from the mean, and where  $L_i^\alpha$  is the longitudinal libration and  $L_i^\beta$  is the latitudinal libration. Here,  $L_i^\alpha$  and  $L_i^\beta$  really measure the position of the lunar pole in the sky with respect to its mean position, so that all the kinds of libration are taken into account. From a least squares fit, we obtain the coefficients  $a_2$  (morning/Grimaldi:  $0.0019 \pm 0.0004$  and evening/Crisium:  $-0.0018 \pm 0.0004$ ) and  $b_2$  (morning/Grimaldi:  $4.2e-5 \pm 0.0003$  and evening/Crisium:  $-0.0003 \pm 0.0004$ ), while  $c_2$  is 1-2 orders of magnitude smaller than  $a_2$ . Since the magnitude of the  $a_2$ ’s are about an order of magnitude greater than the  $b_2$ ’s, the longitudinal libration is more significant than the latitudinal libration. Figure 12 shows the result of fit, and, in particular, that the fit describes the data, in that it can be seen that the observed scattering at this step is mainly accounted for by the libration. For the determination of Figure 12, we used 152 mornings and 168 evenings, and the correlation between the fit and the data is 0.44/0.52 respectively. Using the parameters from the fit, we then normalize the intensities at all lunar phases to the case of zero libration with the equation:

$$I'_i = I_i - (a_2 L_i^\alpha + b_2 L_i^\beta). \quad (25)$$

To check the validity of the libration correction, we performed the libration correction again – but doing it before performing the atmospheric correction described in §5.1. We next performed the atmospheric correction (which still dominates) and the declination correction. At that point, we performed the libration correction again, and we found that  $I_i - \bar{I}_i$  does not have a significant

correlation with the libration. In particular, the parameters from the linear fit of Equation (24) are reduced by an order of magnitude. This test not only confirms the validity of the libration correction performed above, but also guarantees that the three-step corrections can be performed in any order. However, it remains for us to determine the lunar phase function for small phase angles.

#### 5.4. Opposition Effect

To this point, the lunar phase function is incomplete because it is not normalized, and we have not determined its functional form for the smallest phase angles. To do these, we need to know the phase function for small phase angles, and that means that the final lunar phase function for each fiducial patch needs to be normalized to the full moon opposition peak. In reality, the moon is not observable at zero lunar phase because the shadow of the earth would occult the moon, as the earth’s shadow occupies about  $\pm 0.8^\circ$ . So far, the smallest phase we have reached is  $\pm 1.0^\circ$  on the night of November 29, 1993, when a total lunar eclipse occurred over Big Bear. On that night, the sky was clear and stable throughout, and observations were made both before and after the total eclipse, covering lunar phase angles of magnitude ranging between about  $1^\circ$  and  $2^\circ$ , which offers a unique dataset to investigate the slope of the opposition surge effect for all fiducial patches on both the Grimaldi and the Crisium sides.

The images taken during the eclipse were processed and the intensities of the fiducial patches were read out as described in Section 4.1. The atmospheric attenuation has to be corrected to obtain the real moonshine intensity. However, throughout the night, the evolution of the moonshine intensity was controlled not solely by the changing airmass, but also by the changing phase angle. This latter effect is appreciable because of the strong opposition effect at small lunar phase angles. As a result, the shape of the intensity evolution for the two patches deviates strongly from Beer’s law (see Figure 13a and c). Thus, Equation (18) can no longer produce a reasonable fit.

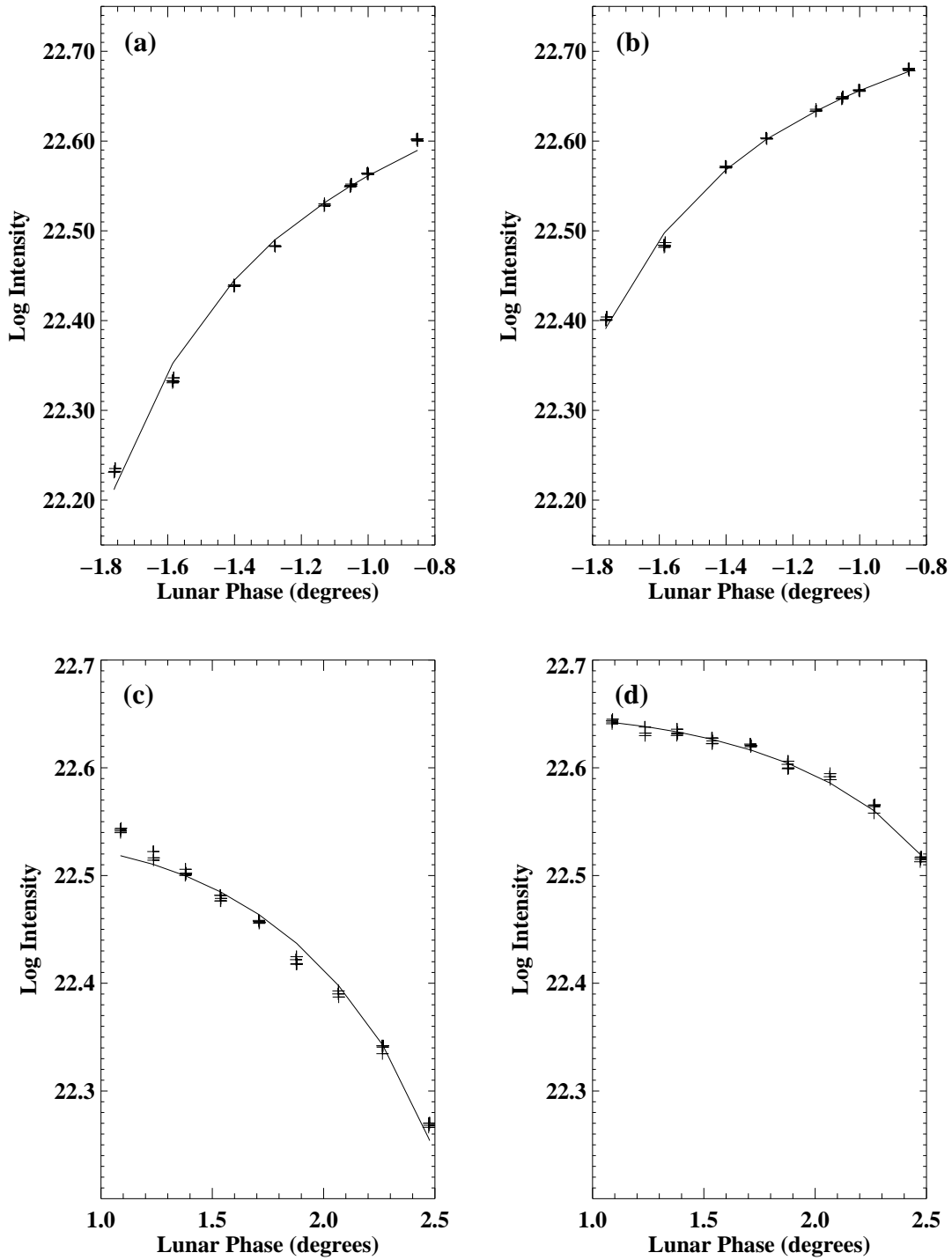


Fig. 13.— Fit of lunar eclipse data obtained on November 29, 1993. (a) Beer’s law fit of the Crisium side (Equation 18); (b) Composite Beer’s law plus opposition effect fit on the Crisium side (Equation 26); (c) same as (a) on the Grimaldi side; (d) same as (b) on the Grimaldi side.

We developed a simple solution to this problem under the reasonable assumption that the opposition effect is linear for very small phase angles, say, from 0 to 5°. During the eclipse, the phase angle changes by less than two degrees for either the Crisium branch or the Grimaldi branch. To determine the slope of the opposition peak for each of the ten fiducial patches, we represent the observed intensity by:

$$I_i = I_0 \times (1 - \gamma|P_i|) \times e^{-\alpha z_i}, \tag{26}$$

where  $I_i$  is the observed intensity at phase angle  $|P_i|$  (in degrees) and airmass  $z_i$ . In contrast to Equation (18),  $I_0$  describes the intensity at both zero airmass and zero phase angle. The second term on the right side describes the linear increase of the phase function as the lunar phase goes to zero. The last term describes the exponential atmospheric attenuation, i.e., Beer’s law, where  $\alpha$  is the atmospheric absorption coefficient for the moonshine.

In applying Equation (26), we used the observed  $I_i$ , after correcting for libration (see §5.3), at lunar phase  $P_i$  and airmass  $z_i$  in Equation (26) above, and made a least-squares, non-linear fit to obtain  $\alpha$ ,  $I_0$ , and the linear opposition effect coefficient,  $\gamma$ . The fit was made for all ten fiducial patches. We did not correct for the declination because the moon is in total eclipse, and that correction should be quite small. We collected about 40 data points for the fit on each side of the moon, i.e., before and after totality, and the standard deviation of the final fit is at the level of 0.5%. Figure 13b and d reveal the improvement in fitting results for one pair of fiducial patches using Equation (26) instead of Equation (18). The improvement is typical of that for all ten patches. From Figure 13, it is also clear that Equation (26) accurately describes the composite effect of the opposition surge and Beer’s law. The fitted opposition peak slope parameter,  $\gamma$ , was

Table 3: Opposition Effect  $\gamma$ ’s, see Equation (26)

Patch	1	2	3	4	5
Grimaldi side	0.084	0.078	0.083	0.079	0.083
Crisium side	0.086	0.079	0.076	0.083	0.083



then used to normalize the phase function for each of the fiducial patches. Figure 14 shows an example of the final lunar phase function normalized to the opposition peak. Of course, each fiducial patch has its own lunar phase function. In detail, for lunar phase of  $5^\circ$  in Figure 14, we used the slope,  $\gamma$ , determined for very small angles to extrapolate to the intensity at zero lunar phase from that at  $5^\circ$ , i.e.,  $I(0) = \frac{I(5)}{1-\gamma \times 5}$ . Then, we normalized that branch of the phase function, its  $\gamma$  and  $I(0)=1$  to fix  $I(5)$ . Combining our knowledge of  $I(5)$  with the relative phase function indicated by the +’s in Figure 14, we obtained the right branch of that figure. The normalization removes the ratio of the geometrical albedos between the two patches, which is restored in Equation (27). The eclipse does not give us data for lunar phases between  $\pm(2^\circ-5^\circ)$ , where we have also assumed a linear form for the phase function. Nights at these small phase angles occur at the fullest of full moons, and we have a few of them. We will enrich our data in this region as time goes on, and can further sharpen our phase function. If there were a systematic error here, it would shift all of our Bond albedos by the same amount. We expect such a systematic error is actually quite small, but we would be able to re-calibrate our present results in the light of future data.

In Table 3, we list the values of the derived opposition coefficients,  $\gamma$ , for all ten fiducial patches. The value of  $\gamma$  for all fiducial patches is approximately 0.08 per degree, indicating that when lunar phase changes from six degrees to zero degrees (full moon), the intensity doubles. This

Table 4:  $\frac{p_a}{p_b}$  (Crisium Side/Grimaldi Side)

Patch	1	2	3	4	5
6	1.121	1.130	1.141	1.086	1.109
7	1.041	1.050	1.060	1.009	1.030
8	0.919	0.926	0.935	0.890	0.909
9	0.983	0.991	1.001	0.953	0.972
10	0.989	0.996	1.006	0.958	0.978

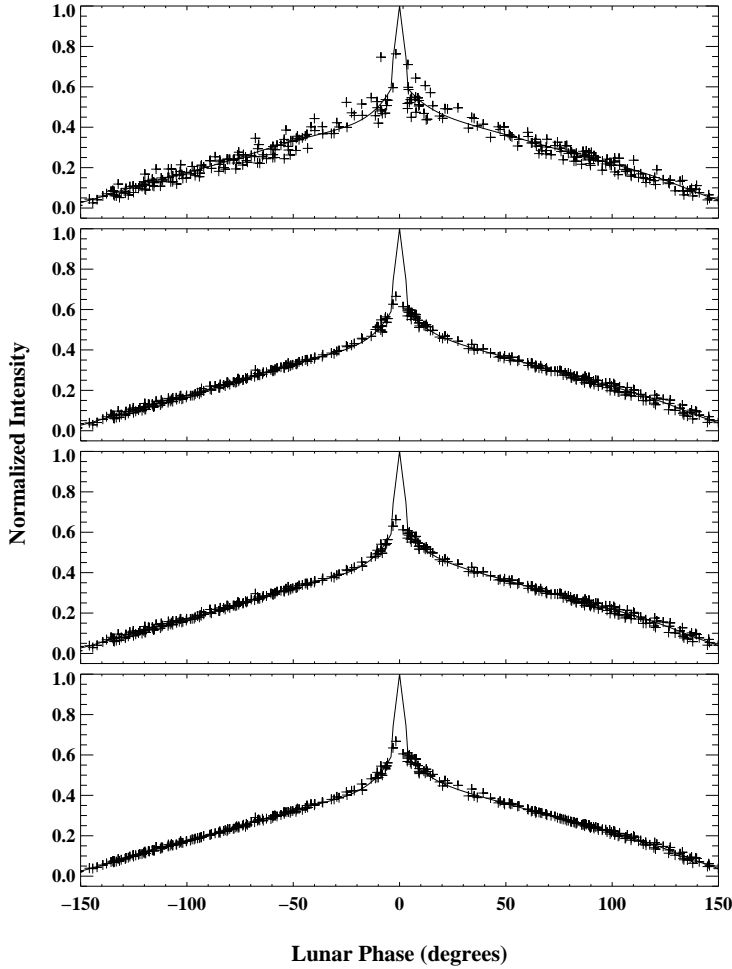


Fig. 14.— The top panel show the apparent, relative lunar phase function from the raw data, for which there are points down to  $2^\circ$ . The function is made relative by normalizing it to unity at phase angle  $0^\circ$ , which means that the ratio of the true right and left branch intensities yields the ratio of the geometrical albedos between Crisium and Grimaldi. The peak near small phase angles represents the opposition effect. Data from a total eclipse are used to connect the positive and negative phase branches of the lunar phase function. No eclipse data are shown in this figure, but the result of the eclipse data is the opposition peak. The second panel from the top shows the result after including correction for the local atmospheric effects using the lunar crescent as a guide star. The third panel also includes the correction for lunar declination. The fourth panel includes the correction for lunar libration. The fit shown in each panel is the final one resulting from all of the corrections described in §5.

is the well-known opposition surge which had not been quantitatively determined previously. The formal error in the determination of  $\gamma$  is about 0.5%.

The parameter  $I_0$  is also used to obtain the ratio of the earthshine patch reflectivity to the moonshine patch reflectivity  $p_a/p_b$ . Table 4 gives the ratios determined between each of the five Crisium patch reflectivities to the each of Grimaldi patch reflectivity.

In Figure 14, we show the lunar phase function with final fit in the lowest panel. The same fit is shown in the other three panels, as well. The points in the top panel represent a normalized version of Figure 10. The second panel shows the result after correction for local atmospheric effects, which is the largest correction. The third and fourth panels show the effects of lunar declination and libration, respectively. The lunar phase function is produced from a fifth degree weighted polynomial fit to the corrected data. After each step of correction, the standard deviation of the fit is reduced from originally 0.05/0.05 (evening/morning) to eventually 0.01/0.01, with the phase function normalized to unity. A restricted regularized fitting is performed as well, which parameterizes the intensities at 181 bins (corresponding to lunar phase  $0^\circ$  to  $180^\circ$ ). These 181 parameters from the fitting describe the lunar phase function, in that the intensity of any lunar phase is the linear interpolation between the values at the two grids into which the lunar phase falls. Note that since there are no data points beyond  $150^\circ$  degrees, the phase function fit beyond this range is not reliable. Similarly, there are not enough data points within  $\pm 5^\circ$ , and so, we used the eclipse data to determine the fitted peak in Figure 14 by treating opposition effect at small phase angles (near the full moon). From the final fit, the estimated error of the mean is at the level of 0.5%; thus, we have measured the lunar phase to 0.5%. How, the phase function in lowest panel of Figure 14 compare with earlier efforts to determine it, like those of Danjon?

In Figure 15, we plot Danjon’s fitted phase function against our corrected one. Danjon used slightly different fiducial patches, but that is not the source of differences, because the phase function shown is about the same for all of our fiducial patches. Rather, the primary source is the opposition surge which was unknown in Danjon’s time. There is a clear offset in the Danjon phase function which would yield uniformly higher albedos than the true phase function. For our

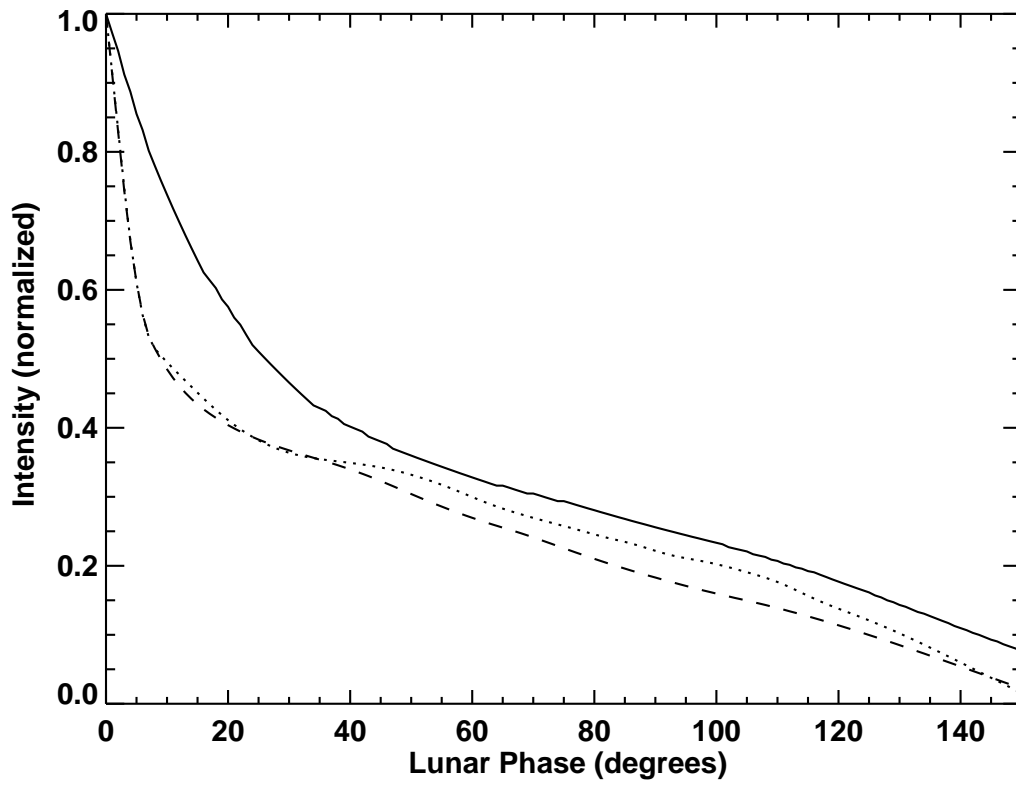


Fig. 15.— Danjon's phase function (solid line) is plotted against lunar phase. Using Figure 14d, the dashed line is our phase function for evening observations and the dotted line for morning for the fiducial patch of Figure 14.

phase function, we have eliminated this erroneous overestimate, by about  $\sim 20\%$ , of the earth’s reflectance introduced by the phase function in earlier incarnations of earthshine studies, like those of Danjon.

## 6. Precision of the Determination of the Earth’s Nightly Albedo

The effective albedo is calculated from the earthshine measurement by combining equations (9) and (17):

$$A^*(\beta) = \frac{3}{2f_L} \frac{p_b f_b(\theta)}{p_a f_a(\theta_0)} \frac{I_a/T_a}{I_b/T_b} \frac{R_{em}^2}{R_e^2} \frac{R_{es}^2}{R_{ms}^2}, \quad (27)$$

where  $\frac{I_a/T_a}{I_b/T_b}$  is the ratio of the earthshine intensity to the moonshine intensity in two opposing fiducial patches, after correcting for airmass. The ratio between the physical reflectivity of the two opposing fiducial patches,  $\frac{p_b}{p_a}$ , is determined from the lunar eclipse data taken at BBSO on November 29, 1993, as discussed in Section 5.4. The lunar phase function for the bright side,  $f_b(\theta)$ , is used in the formula to account for the geometrical dependence of the reflectivity of the moon, while  $f_a(\theta_0)$  accounts for the fact that the earthshine is not exactly retroreflected from the moon ( $\theta_0 \lesssim 1^\circ$ ). In our analysis,  $\theta_0$  is taken as the angle between the observer’s position and the mean of the sub-solar point (position on the earth’s surface of the solar zenith) and the sub-lunar point (position on the earth’s surface of the moon’s zenith) with the apex of the angle being defined with respect to the fiducial patch under consideration, see Figure 1. We assume that the moonshine and earthshine have the same lunar phase function for each fiducial patch. Thus, we take  $f_a(\theta_0)$  from the appropriate moonshine phase function. The earthshine is slightly bluer than the moonshine because of Rayleigh scattering by the earth’s atmosphere. This small effect is subsumed in the lunar geometrical albedos.

From Equation (27), one may surmise that the observational errors arising from measuring  $A^*$  from two opposing fiducial patches come from the errors in the readout intensity from the moonshine and earthshine fiducial patches, the error in the transmission of the BS filter (about 0.8%), and the error in the determination of lunar phase function. The ratio  $\frac{p_b}{p_a}$  can be regarded

as the relative normalization of the phase functions of the opposing fiducial patches. The standard deviation of the lunar phase function can be determined down to 0.5% from a co-variance calculation with a comparable uncertainty for the ratio  $\frac{p_b}{p_a}$ . The standard deviation of the Beer’s law fitting of the moonshine for each night is taken as the error of the moonshine intensity. This gives a value of 1.1%. For the case of the earthshine, the scattering of the data is due to both the noise and the real physical changes in the terrestrial albedo. The average standard deviation from Beer’s law fitting of the earthshine intensities is 1.9%. Conservatively speaking, if half the amount of such scattering comes from the real physical change on average, the error in nightly earthshine intensity measurement is about 1.0%. Adding up all the errors and assuming they are independent, we get a nightly measurement error of nearly 2%. If one regards the measurements from different pairs as being independent, the 2% is reduced to about 1%. If we combine nights to obtain, say, a seasonal average, then the total error will be smaller, but no smaller than that associated with the mean values of the various lunar phase functions and their relative normalizations. We regard the determination of the ratio  $\frac{p_b}{p_a}$  as being the most likely source of systematic errors. Measurements of the opposition effect in future eclipses will allow us to determine if there are systematic errors, and correct the albedos in retrospect.

To determine the Bond albedo,  $A$ , from our earthshine observations we need to integrate  $A^*(\theta)$  over all phases of the moon. Combining Equations (5), (6) and (8), we find

$$A = \frac{2}{3} \int_{-\pi}^{\pi} d\theta A^*(\theta) f_L(\theta) \sin \theta. \quad (28)$$

There are two basic problems using this approach to determine the Bond albedo. The first, and more significant problem, is that we cannot measure the earthshine for all phases of the moon. This becomes a problem primarily for lunar phases near the new moon, where the earth is most nearly Lambertian. The second basic problem in using the earthshine to determine the albedo arises because the orbit of the moon traces out an ellipse in the full three dimension space surrounding the earth, so we cannot measure the earthshine in all directions. Therefore, we are insensitive to any azimuthal anisotropy in the earthshine. In the subsequent papers, we

will demonstrate that the anisotropy is not significant, and one can account for it. We do this by taking advantage of full spatial coverage provided by the simulations. For the first problem, we will show that we can obtain a quite reliable Bond albedo from the earthshine data. These are among the subjects of Paper II of this series.

This research was supported in part by a grant from NASA (NAG5-11007).

## REFERENCES

- C. W. Allen, 1973, *Astrophysical Quantities*, p.125
- Buratti et al., 1997.
- Flatte, S., Koonin, S., and MacDonald, G., 1991, in *Global Change and the Dark of the Moon*, JSR-91-315 (McLean, VA: The MITRE Corporation)
- Danjon, A., 1928, *Ann. Obs. Strasbourg*, 2, 165
- Danjon, A., 1954, in *The Earth as a Planet*, ed. Kuiper, p.726, Chicago
- Dubois, J., 1947, *Bull. Astron.*, 13, 193
- Franklin, F.A., 1967, *J.Geophys.Res.*, 72, 2963
- Fritz, S., 1949, *J. Meteor.*, 6, 277
- Fröhlich, C., 2000, *Observations of irradiance variations*, *Space Science Reviews*, v. 94, 15.
- Goode PR, Qiu J, Yurchyshyn V, Hickey J, Chu MC, Kolbe E, Brown CT, Koonin SE, 2001, Earthshine observations of the earth's reflectance, *Geophys. Res. Lett.*, 28 (9), 1671-1674.
- Hapke, B., *Physics and Astronomy of the Moon*, 2nd edition, ed. Z. Kopal (Academic Press, New York, 1971), 155
- Huffman, D., Weidman, C. and Twomey, S., 1990, *Colloq Andre Danjon, Jounees 1990, Capitaine and Detarbat*, eds. (Paris: Paris Observatory), p. 111
- Kennedy, J.R., 1969, M.S. Thesis, Fresno State College, unpublished
- Lean, J., 1997, The sun's variable radiation and its relevance for earth, *Ann. Rev. Astron.*, 35, 33
- Ram, M. and Stoltz, M.R., 1999, Possible solar influences on the dust profile of the GISP2 ice core from Central Greenland, *Geophys. Res. Lett.*, 26, No. 12, 1763
- Willson, R.C. and Hudson, H.S., 1988, Solar luminosity variations in solar cycle-21, *Nature*, 332, 810



Willson, R.C. and Hudson, H.S., The suns luminosity over a complete solar-cycle 1991, *Nature*,  
351, 42